# Chapter IV: Higher-order cellular information processing using synthetic RNA devices*


## Abstract

The engineering of biological systems is critical to developing effective solutions to many societal challenges including energy and food production, environmental quality, and health and medicine. Programmed cellular information processing and control devices are needed to engineer biological systems[1]. Here, we demonstrate synthetic RNA devices that perform a variety of higher-order cellular information processing operations, including logic (AND, NOR, NAND, OR gates), signal filters, and signal gain (cooperativity). RNA devices process and transmit molecular input signals to targeted protein level outputs, linking computation and logic to gene expression and thus cellular function. The devices are assembled from modular RNA components through a first-generation composition framework, highlighting the potential of such synthetic biology strategies to support the rapid engineering of cellular behavior.



*Reproduced with permission from: M. N. Win and C. D. Smolke. (2008) Manuscript submitted.

## 4.1. Introduction

Our ability to transmit information to and from living systems and to act on information inside living systems is critical to advancing the scale and complexity at which we can engineer, manipulate, and probe biological systems. There is a need for higher-order cellular information processing and control devices that produce new cellular functions from the diverse molecular information present within biological systems, such as small molecules, proteins, and RNA. For example, logic operations that process and translate multiple molecular inputs into prescribed levels of new molecular outputs are critical to a cell's ability to integrate diverse environmental and intracellular signals to a smaller number of phenotypic responses. As another example, basic computation operations such as signal gain, amplification, restoration, and filtering enable useful manipulation of molecular information through cellular networks.

Researchers have demonstrated many examples of molecular information processing systems that perform computation and logic with biological substrates. For example, protein-based systems that perform logic operations to convert molecular inputs to the regulation of transcriptional events have been demonstrated[2-5]. However, systems based on protein components have faced limitations in the molecular inputs that can be processed, programmability of the components themselves, functional dependence on cell-specific machinery, and the variety of information processing operations that can be readily obtained. As a second example, inspired by the diverse functions exhibited by nucleic acids[6] and the predictability of Watson-Crick base pairing interactions, researchers have built many *in vitro* information processing systems comprised of nucleic acid components, including DNA computing machines that implement logic operations and signaling cascades based solely on

nucleic acid hybridization events[7, 8], molecular automata comprised of deoxyribozymes regulated by nucleic acid inputs that perform various computation and logic functions[9-11], and molecular computers that utilize protein enzymes to regulate sequence-specific cleavage and joining of nucleic acids[12, 13]. Allosteric ribozymes that implement logic functions in response to small molecule[14, 15] and nucleic acid[16, 17] inputs have also been demonstrated *in vitro*.

Significantly, researchers have constructed a variety of single-input RNA switches that process nucleic acid and small molecule inputs to regulate gene expression events *in vivo*[18, 19]. RNA-based systems that integrate multiple RNAi substrates for combinatorial regulation of gene expression i*n vivo* have also been demonstrated [20, 21]. However, an important next challenge is to combine the inherent richness that nucleic acid substrates possess for performing information processing and control operations with the design advantages expected from the relative ease by which RNA structures can be modeled and thus designed, as compared to proteins[22, 23]. Incremental progress towards overcoming this challenge would allow many new generic devices to be engineered, which operate reliably inside living cells, provide access to otherwise inaccessible information of cellular state, and allow sophisticated exogenous and embedded control of cellular functions.

## 4.2. Results

### *4.2.1. Functional RNA device composition framework and general signal integration schemes*

We recently described a framework for the construction of single input/output RNA devices[24] that is based on the modular assembly of three functional components: a sensor component, comprised of an RNA aptamer; an actuator component, comprised of a

hammerhead ribozyme[25]; and a transmitter component, comprised of a sequence that couples the sensor and actuator components. The transmitter component utilizes competitive hybridization events to enable design of conformational changes that are linked to functional states of the molecule. The proposed framework is also based on the modular coupling of the RNA device and the target genetic construct through the 3' untranslated region (UTR), where self-cleavage inactivates the transcript independent of cell-specific machinery. From this early framework, we demonstrated simple RNA devices that function as single-input gene expression ON and OFF switches (here referred to as Buffer and Inverter gates, respectively), which convert both cellular and exogenous molecular inputs to regulated gene expression via input-dependent regulation of ribozyme activity[24].

In engineering design, the utility of a proposed composition framework depends, in part, on the extensibility of the framework itself. We hoped to demonstrate that our careful specification of defined points of integration, or 'nodes', could be used to facilitate the assembly of putatively modular RNA components into more sophisticated cellular information processing devices (Figure 4.1A). Thus, here, we describe an extended framework for engineering higher-order RNA devices, based on three signal integration (SI) schemes that correspond to different modes of assembly for device components (Figure 4.1B). The first signal integration scheme (SI 1) is used to construct RNA devices that perform logic (AND, NOR gates) and bandpass signal filter operations through the assembly of independent single-input gates in the 3' UTR. The second integration scheme (SI 2) is used to construct devices that perform other logic operations (NAND, OR gates) through the assembly of two individual sensor-transmitter components linked to both stems of the ribozyme. The third scheme (SI 3) is used to construct devices that perform logic (AND, OR

gates) and signal gain (cooperativity) operations through the assembly of two individual sensor-transmitter components linked to a single ribozyme stem.

**A** **Functional composition of an RNA device**

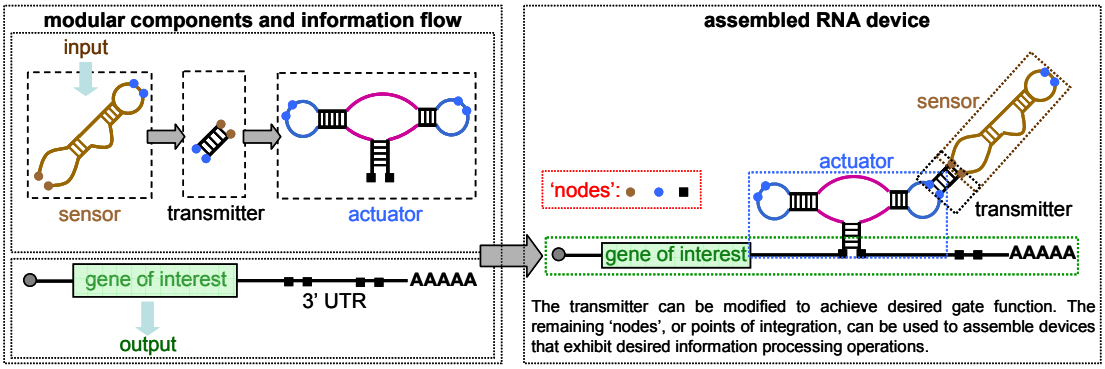


**B** **Signal integration (SI) schemes**

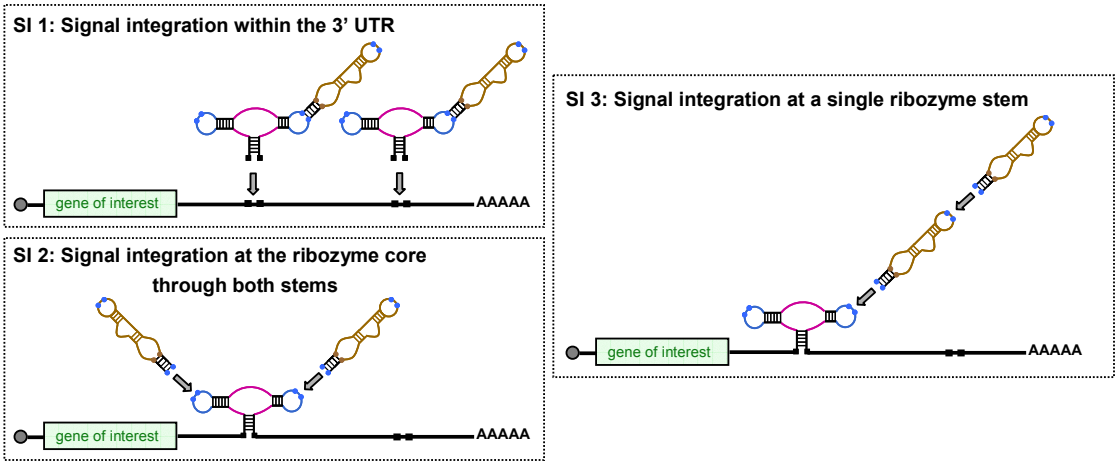


**Figure 4.1.** Functional RNA device composition framework. Color schemes follow those previously described[24]: brown, aptamer or sensor component; purple, catalytic core of the ribozyme or actuator component; blue, loop regions of the actuator component; green and red, competing and switching strands of the transmitter component, respectively. (A) Schematics of the functional composition framework for assembling RNA devices. An RNA device is composed of three modular components: a sensor, a transmitter, and an actuator. Information in the form of a molecular input is received by the sensor and transmitted by the transmitter to a regulated activity of the actuator, which in turn controls the target expression level as an output. Nodes specify physical points of integration between components through which devices are assembled. (B) Schematics of three primary signal integration schemes representing different component assembly strategies to build higher-order RNA devices. The RNA device in SI 1 involves multiple actuator components controlled by single sensor-transmitter components, whereas those in SI 2 and 3 involve multiple sensor-transmitter components controlling a single actuator component. The mode of assembly determines the mechanism of signal integration as highlighted by the coupled nodes.

### *4.2.2. Higher-order RNA device based on SI 1 (signal integration within the 3' UTR)*

Different information processing operations are implemented through SI 1 by altering the function (Buffer, Inverter) and input responsiveness of the coupled single-input gates. The single-input gates act independently and therefore computation is performed through the integration of individual gate actions in the 3' UTR of the target transcript. We constructed a set of higher-order RNA devices by coupling representative Buffer or Inverter gates[24] responsive to either theophylline or tetracycline (SI 1.1; Figure 4.2A). The coupled same-input gate device has a naturally-occurring functional counterpart composed of two distinct riboswitches responsive to the same metabolite, thiamine pyrophosphate (TPP)[26]. By coupling two functionally identical single-input gates that are responsive to the same molecular input, a signal shift in the device response, or output swing, was observed from the coupled device compared to that of the single-input gate response, confirming the independent action of each gate (Figure 4.2B, Supplementary Text 4.1 and 4.2, Supplementary Table 4.1). This information processing operation can be used to program the output swing and basal output signal of a given single-input device to match the desired threshold values for a particular application.

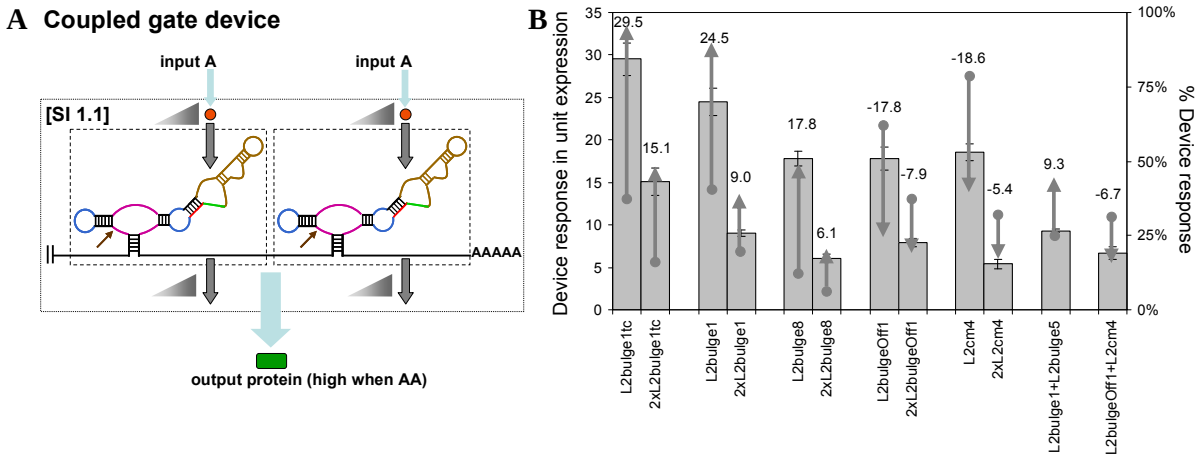

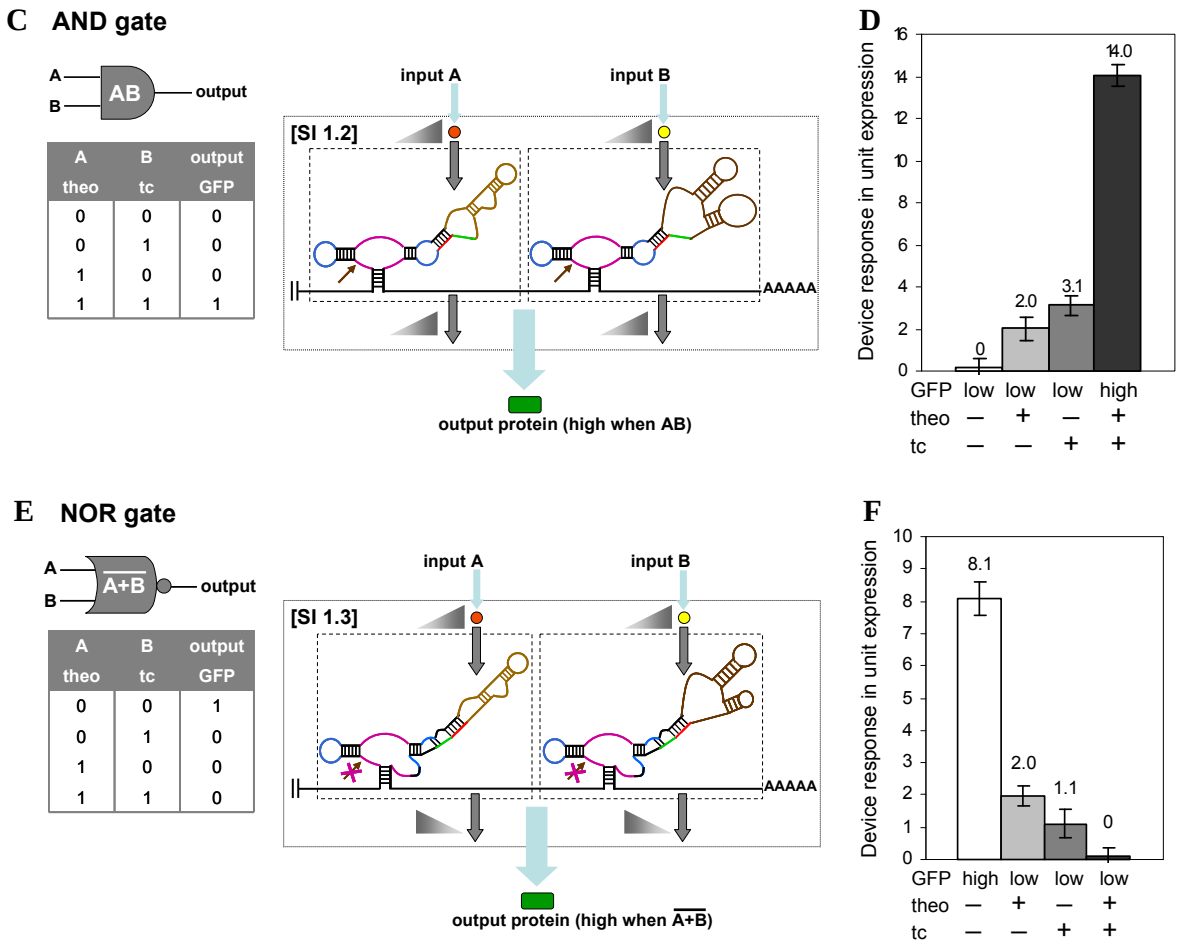


**Figure 4.2.** Higher-order RNA devices based on signal integration within the 3' UTR (SI 1). Color schemes follow those described in Figure 4.1. Each single-input gate is indicated in a boxed region, and triangles indicate relationships between associated gate inputs and outputs. (A) Schematic representation of an RNA device comprised of two Buffer gates responsive to the same input molecule. The RNA device functions to shift the output swing from that of the single-input gate. (B) The device response of RNA devices comprised of two single-input gates and their single-input gate counterparts. Device response (bars) is reported as the output swing in units of expression as described in Materials and Methods and the corresponding percent device response (arrows) is reported over the full transcriptional range of the employed promoter system. Output swings are reported from 0 mM to 10 mM theophylline and 0 mM to 1 mM tetracycline. The negative sign indicates the down-regulation of target gene expression by the Inverter gates. (C) Schematic representation of an RNA device that performs an AND gate operation by coupling two Buffer gates responsive to different input molecules and the associated truth table. (D) The device response of an AND gate operator (L2bulge1+L2bulge1tc). Device response under different input conditions (theo or tc (-), 0 mM; theo (+), 5 mM; tc (+), 0.25 mM) is reported as the output swing in units of expression relative to the absence of both inputs as described in Materials and Methods. (E) Schematic representation of an RNA device that performs a NOR gate operation by coupling two Inverter gates responsive to different input molecules and the associated truth table. (F) The

device response of a NOR gate operator (L2bulgeOff1+L2bulgeOff1tc). Device response under different input conditions (theo or tc (-), 0 mM; theo (+), 10 mM; tc (+), 0.5 mM) is reported as in (D), except that output swings are reported relative to the presence of both inputs.

We next constructed a higher-order RNA device that performs an AND gate operation by coupling a theophylline-responsive Buffer gate (L2bulge1[24]) and a tetracycline-responsive Buffer gate (L2bulge1tc[24]) in the 3' UTR (SI 1.2; Figure 4.2C). In the absence of the molecular inputs (theophylline or tetracycline), both Buffer gates favor the 'ribozyme-active' state, a conformation that results in transcript cleavage and low device output (low gene expression levels). In the presence of either input, one of the single-input gates remains in the ribozyme-active state and device output remains low. Device output is substantially increased only when both molecular inputs are present (Figure 4.2D). Similar to other molecular systems that perform cellular logic operations[27], the RNA devices reported here exhibit non-digital logic. We constructed a second RNA device that performs an AND gate operation by coupling L2bulge1tc and a different theophylline-responsive Buffer gate (L2bulge9[24]) to demonstrate the generality of SI 1 for constructing AND gate operators with different single-input gates (Supplementary Figure 4.1).

We constructed another higher-order RNA device that performs a NOR gate operation by coupling a theophylline-responsive Inverter gate (L2bulgeOff1[24]) and a tetracycline-responsive Inverter gate (L2bulgeOff1tc; Supplementary Figure 4.2) in the 3' UTR (SI 1.3; Figure 4.2E). The coupled different-input Inverter gate device has a naturally-occurring functional counterpart composed of two distinct riboswitches, responsive to respective metabolites coenzyme $B_{12}$ and S-adenosylmethionine, in which the regulated gene expression output is low in the presence of either metabolite or both, thereby functioning as a

NOR gate operator[27]. Similarly, in the absence of the molecular inputs, both Inverter gates in our engineered device favor the 'ribozyme-inactive' state, a conformation that results in reduced transcript cleavage and high device output. In the presence of either input, one of the single-input gates favors the ribozyme-active state and device output is lowered. Device output is more effectively lowered when both inputs are present, as both single-input gates favor ribozyme-active states (Figure 4.2F). We also constructed a second NOR gate operation by coupling L2bulgeOff1 to a different tetracycline-responsive Inverter gate (L2bulgeOff2tc; Supplementary Figure 4.2) in order to demonstrate the generality of SI 1 for constructing NOR gate operators with different single-input gates (Supplementary Figure 4.3).

We next constructed an RNA device that performs a bandpass filter operation by coupling theophylline-responsive Buffer and Inverter gates (L2bulge1 and L2bulgeOff1) in the 3' UTR (SI 1.4; Supplementary Figure 4.4). In the absence of the molecular input, the Buffer gate favors the ribozyme-active state, resulting in low device output. However, in the presence of the input, the Inverter gate favors the ribozyme-active state, also resulting in low device output. Only over intermediate input concentration ranges do both single-input gates favor a ribozyme-inactive state, resulting in higher device output. Therefore, diverse cellular computation and logic operations can be constructed through SI 1, where layering strategies may be used to extend device designs to other information processing operations (Supplementary Text 4.3).

### *4.2.3. Higher-order RNA devices based on SI 2 (signal integration at the ribozyme core)*

Different information processing operations are implemented through SI 2 by altering the function and input responsiveness of the coupled sensor-transmitter components (Figure

4.1B). The sensor-transmitter components act independently through the linked ribozyme stems and therefore computation is performed through the integration of individual sensor-transmitter actions in the ribozyme core of the RNA device. An independent sensor-transmitter component is indicated as an internal Inverter gate if the presence of input results in activation of the coupled component, such as an actuator or another internal gate. Similarly, an internal Buffer gate indicates a sensor-transmitter component that results in inactivation of the coupled component in the presence of input.

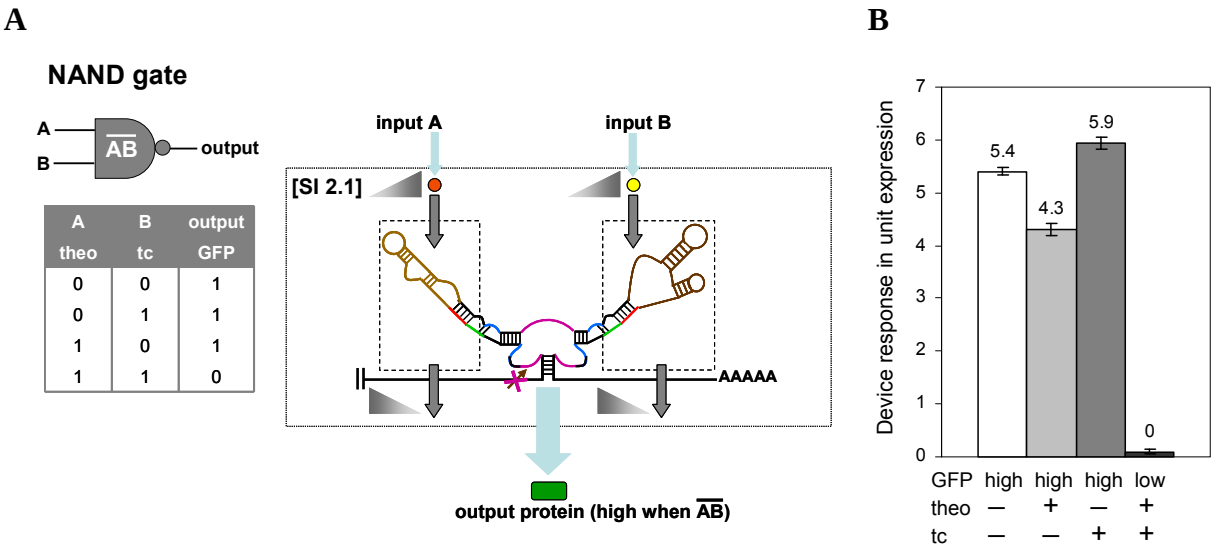


**Figure 4.3.** Higher-order RNA devices based on signal integration at the ribozyme core (SI 2). Color schemes follow those described in Figure 4.1. Each internal gate, comprised of a sensor-transmitter component, is indicated in a boxed region, and triangles indicate relationships between associated internal gate inputs and outputs. (A) Schematic representation of an RNA device that performs a NAND gate operation by coupling two internal Inverter gates responsive to different input molecules to different ribozyme stems and the associated truth table. (B) The device response of a NAND gate operator (L1cm10-L2bulgeOff3tc). Device response under different input conditions (theo or tc (-), 0 mM; theo (+), 10 mM; tc (+), 1 mM) is reported as in Figure 4.2F.

We constructed a higher-order RNA device that performs a NAND gate operation by coupling a theophylline-responsive internal Inverter gate (L1cm10[24]) through stem I and a tetracycline-responsive internal Inverter gate (L2bulgeOff3tc; Supplementary Figure 4.2) through stem II (SI 2.1; Figure 4.3A). In the absence of the molecular inputs, both internal Inverter gates and hence the RNA device, favor the ribozyme-inactive state, resulting in high device output. In the presence of either input, one of the internal Inverter gates remains in the ribozyme-inactive state and the device output remains high. The RNA device only favors the ribozyme-active state, resulting in low device output, when both molecular inputs are present (Figure 4.3B). We constructed a second RNA device that performs a NAND gate operation by coupling L1cm10 and a different tetracycline-responsive internal Inverter gate (L2bulgeOff1tc; Supplementary Figure 4.2) in order to demonstrate the generality of SI 2 for constructing NAND gate operators with different sensor-transmitter components (Supplementary Figure 4.5). By altering the function of the coupled sensor-transmitter components, other logic operations can be constructed through SI 2, such as an OR gate operation through the coupling of two internal Buffer gates (Supplementary Text 4.4).

### *4.2.4. Higher-order RNA devices based on SI 3 (signal integration through a single ribozyme stem)*

In SI 3 different information processing operations are constructed through the coupling of multiple sensor-transmitter components through one stem of the ribozyme (Figure 4.1B). Here, the actions of the sensor-transmitter components are coupled, with computation occurring via the integrated action of the internal gates within a single ribozyme stem. Internal gates are linked through the aptamer loop of the lower gate, IG(n), to the transmitter sequence of the higher gate, IG(n+1), where the state of the internal gate adjacent

to the ribozyme (IG1) determines the state of the RNA device. We constructed a second type of higher-order RNA device that performs an AND gate operation by coupling a theophylline-responsive internal Buffer gate (IG1) and a tetracycline-responsive internal Inverter gate (IG2) at stem II (SI 3.1; Figure 4.4A). In the absence of both molecular inputs or the presence of input to IG1, the RNA device favors the ribozyme-active state, resulting in low device output. In the presence of the molecular input to IG2, although the state of IG2 changes, the RNA device remains in the ribozyme-active state and the device output remains low. Only in the presence of both molecular inputs do the states of both internal gates change and the RNA device favors the ribozyme-inactive state, resulting in high device output (Figure 4.4B). We constructed two other RNA devices through SI 3 that perform AND gate operations to demonstrate the generality of the assembly scheme for constructing AND gate operators with different internal gates (Supplementary Figure 4.6). We also constructed RNA devices that perform OR gate operations through SI 3 (Supplementary Text 4.4).

We used SI 3 to examine the design strategies for RNA devices that perform signal gain operations, or programmed cooperativity. We constructed RNA devices that perform signal gain by coupling theophylline-responsive internal Buffer (IG1) and Inverter (IG2) gates (SI 3.2; Figure 4.4C). The sensor-transmitter components of the RNA device can be programmed to bind inputs in a cooperative manner by manipulating the relative energies required to switch the device between different states (programmed through the transmitter components). Functional characteristics of cooperative ligand-binding regulatory systems typically involve a larger change in the response properties transiting from a low-affinity state to a high-affinity state as more ligands occupy the available binding sites, and are quantitatively represented by Hill coefficients ($n_H$) greater than one[28].

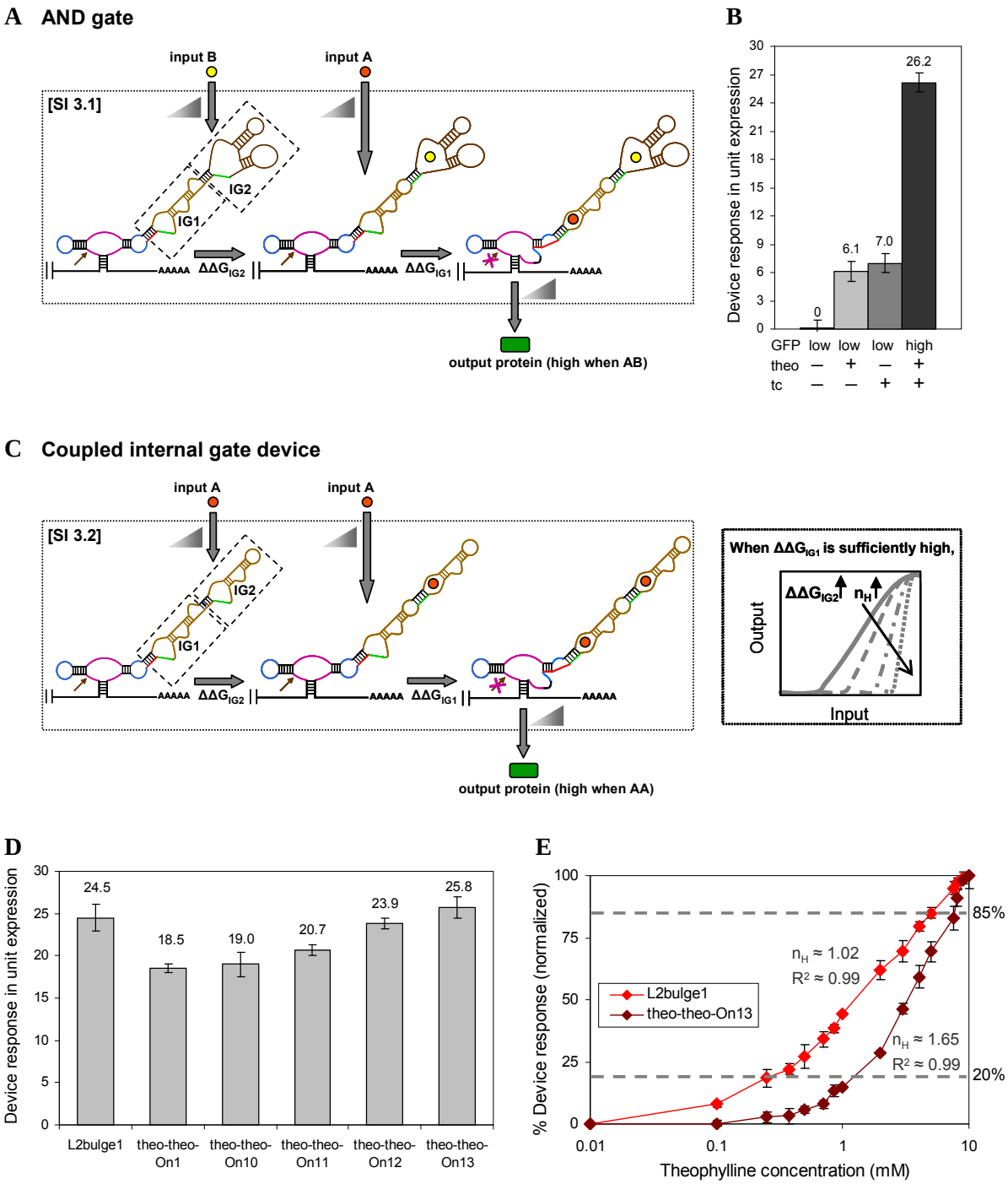


**Figure 4.4.** Higher-order RNA devices based on signal integration at a single ribozyme stem (SI 3). Color schemes follow those described in Figure 4.1. Each internal gate (IGn), comprised of a sensor-transmitter component, is indicated in a boxed region, and triangles indicate relationships between associated internal gate inputs and device outputs. The three states that the device can adopt and associated free energy changes between each state are illustrated. (A) Schematic representation of an RNA device that performs an AND gate operation by coupling internal Buffer (IG1) and Inverter (IG2) gates responsive to different

input molecules to a single ribozyme stem. (B) The device response of an AND gate operator (tc-theo-On1). Device response under different input conditions (theo or tc (-), 0 mM; theo (+), 2.5 mM; tc (+), 0.5 mM) is reported as in Figure 4.2D. (C) Schematic representation of an RNA device comprised of internal Buffer (IG1) and Inverter (IG2) gates responsive to the same input molecule coupled to a single ribozyme stem. (D) The device response of RNA devices comprised of internal Buffer and Inverter gates and their single-internal gate device counterpart (L2bulge1). Device response is reported as in Figure 4.2B. Theo-theo-On10 – 13 are devices that exhibit varying levels of signal gain. (E) The device response of theo-theo-On13 shows a high degree of programmed cooperativity compared to that of L2bulge1. The percent device response is plotted by normalizing corresponding dynamic switching ranges between the absence and presence of 10 mM theophylline to 0-100% as described in Materials and Methods.

We first engineered a series of nine RNA devices, in which the sequences within the IG2 transmitter component were altered to modify the energetic differences between the first and second states ($\Delta\Delta G_{IG2}$), while keeping the energetic differences between the second and third states constant ($\Delta\Delta G_{IG1}$ = 0.3 kcal/mol) (Supplementary Table 4.2). All nine RNA devices function as Buffer gates similar to L2bulge1 (Supplementary Figure 4.7); however, none of the devices exhibited gain in their output response ($n_H \approx 1$) (Supplementary Figure 4.8). This suggests that the energy required to switch between the second and third states ($\Delta\Delta G_{IG1}$; programmed into IG1 transmitter component) may play a critical role in simulating different effective binding affinities between IG1 and IG2 that will result in a signal gain operation (Supplementary Text 4.5). Therefore, we constructed a second series of RNA devices in which the energetic difference between the second and third states is increased ($\Delta\Delta G_{IG1}$ = 1 kcal/mol; Supplementary Table 4.2). All four devices function as Buffer gates (Figure 4.4D) and exhibited substantial levels of gain in the output response as indicated by Hill coefficients greater than 1 (Supplementary Figure 4.9), where theo-theo-On13 exhibited the highest signal gain ($n_H \approx 1.65$) (Figure 4.4E) and a similar degree of cooperativity as the naturally-occurring glycine riboswitch[29]. In general, the degree of programmed cooperativity ($n_H$) was positively correlated with $\Delta\Delta G_{IG2}$ values. We also constructed a series of RNA

devices in which internal Inverter gates were placed into IG1. All eight devices function as Inverter gates similar to L2bulgeOff1 (Supplementary Figure 4.10), and one of these devices (theo-theo-Off6) exhibited slight signal gain ($n_H \approx 1.2$) (Supplementary Figure 4.11). Mutational studies validated that the device response and signal gain operation is achieved through binding of the molecular input to both sensor components (Supplementary Figures 4.12-4.15).

### 4.3. Discussion

Functional composition frameworks that support the programming of complex devices through the modular assembly of distinct components are important foundations to engineering design[1]. Such frameworks support the efficient and reliable engineering of diverse device functions from well-characterized components without complex device redesign. We have developed a first-generation composition framework for constructing higher-order RNA devices. Functional modularity is a critical element of any composition framework and achieved in part here through the separation of device functions (sensing, actuation, and information transmission) into distinct components. Rational modular assembly is achieved by controlling information transmission between the sensing and actuation components through hybridization interactions. Therefore, while the functions of sensing and actuation frequently rely on more complex tertiary interactions, which are not accounted for in this first-generation framework, the integration of these functions into an RNA device is simplified via a transmitter that acts to both insulate component functions and control the interactions between components through predictive secondary structure interactions.

Besides the utility of the devices themselves, the variety of cellular information processing operations demonstrated here contributes important validation for our modular assembly and rational design approach. In addition, the framework may be further extended to more complex devices by combining the proposed signal integration schemes (SI 1, 2, and 3) within an RNA device. Future efforts leading to new device designs that enable other computation, such as signal restoration and amplification, will be critical to the extension to more complex information processing schemes.

The integration of future scientific and technological advances with the design approaches presented here, should lead to improved, next-generation frameworks for more reliable and robust assembly of RNA devices. For example, scientific advances that lend further insight into RNA structure-function relationships[30], and improve predictions of RNA secondary and tertiary structures relevant to *in vivo* folding environments[23], will allow for the development of improved modular assembly schemes, where the insulation of device functions across distinct components and controlled interaction between these components remains a design challenge. As a second example, the development of modeling tools that can predict both thermodynamic and kinetic properties of RNA folding *in vivo*[22], incorporate tertiary interactions, and link those properties to functional states and gene expression pathways will support future design tools that efficiently optimize and program device properties *in silico*. As a third example, technological advances that allow for the efficient generation of well-characterized libraries of sensor components, RNA aptamers[31, 32], that recognize biologically-relevant molecules, function in the cellular environment, and are compatible with the composition frameworks will be critical to the broader implementation of RNA devices toward user-specified processing of environmental and intracellular signals.

Taken together, the thoughtful combination of scientific research and engineering theory will allow still more sophisticated RNA devices to be developed. The resulting improvements in our ability to transmit information to and from living systems, and implement control within cells themselves, will transform how we interact with and program biology.

## 4.4. Materials and Methods

### *4.4.1. Plasmid construction, cloning, and cell strains*

Using standard molecular biology techniques[33], the plasmid pRzS, harboring the yeast-enhanced green fluorescence protein (yEGFP)[34] under the control of a GAL1-10 promoter, was constructed as previously described[24] and employed as a universal vector for the characterization of all higher-order RNA devices. All RNA device constructs were generated by PCR amplification using the appropriate oligonucleotide templates and primers. All oligonucleotides were synthesized by Integrated DNA Technologies (IDT). Single ribozyme devices (SI 2 and 3) were cloned into two unique restriction sites, *Avr*II and *Xho*I, 3 nucleotides downstream of the stop codon of yEGFP and upstream of an ADH1 terminator sequence. For dual ribozyme devices (SI 1), the second single-input gate including spacer sequences was cloned immediately downstream of the first single-input gate in the second restriction site (*Xho*I). Sequences of all devices are available in Supplementary Text 4.6. Representative secondary structures and sequences are illustrated in Supplementary Figures 4.16 and 4.17. Cloned plasmids were transformed into an electrocompetent *Escherichia coli* strain, DH10B (Invitrogen) and all ribozyme constructs were confirmed by subsequent sequencing (Laragen, Inc). Confirmed plasmid constructs were transformed into a

*Saccharomyces cerevisiae* strain (W303 *MATα his3-11,15 trp1-1 leu2-3 ura3-1 ade2-1*) using standard lithium acetate procedures[35].

### *4.4.2. RNA secondary structure prediction, free energy calculation, and corresponding proposed mechanism*

RNAstructure 4.2 (http://rna.urmc.rochester.edu/rnastructure.html) was used to predict the secondary structures of all RNA devices and their corresponding thermodynamic properties as previously described[24]. Prediction of the secondary structures of the RNA devices based on SI 1 and 2 have been previously described[24]. RNA sequences that are predicted to adopt at least two stable equilibrium conformations (ribozyme active and inactive) were constructed and characterized for their functional activity. Our design strategy is based on the conformational dynamics characteristic of RNA molecules that enables them to distribute between these two different conformations: one in which the competing strand is not base-paired or base-paired such that the ligand-binding pocket is not formed, and the other in which the competing strand is base-paired with the aptamer (sensor) base stem, displacing the switching strand and thus allowing the formation of the ligand-binding pocket. Strand displacement results in the disruption (Buffer gate) or restoration (Inverter gate) of the catalytic core of the actuator ribozyme. Binding of input to the latter conformation shifts the equilibrium distribution to favor the input-bound form as a function of increasing input concentration. For RNA devices comprised of two internal gates (SI 3), RNA sequences that are predicted to adopt generally at least three stable equilibrium conformations of interest, as illustrated in Figure 4.4A and 4.4C, were constructed and characterized for their functional

activity. The device design strategies and their regulatory mechanisms closely follow those described above.

### *4.4.3. In vivo assays for characterization of RNA device properties and fluorescence quantification*

As previously described[24], *S. cerevisiae* cells harboring plasmids carrying appropriate RNA devices were grown in synthetic complete medium supplemented with an appropriate amino acid dropout solution and sugar (2% raffinose, 1% sucrose) overnight at 30$^{o}$C. The overnight cell cultures were back-diluted into fresh medium to an $OD_{600}$ of approximately 0.1. At the time of back-dilution, an appropriate volume of galactose (2% final concentration) or an equivalent volume of water were added to the cultures for the induced and non-induced controls, respectively. In addition, an appropriate volume of concentrated input stock dissolved in medium, or an equivalent volume of the medium (no input control) was added to the cultures (to the appropriate final concentration of theophylline, tetracycline, or both inputs, as described in the figure legends). The back-diluted cells were then grown to an $OD_{600}$ of 0.8-1.0 or for a period of approximately 6 hours before measuring output GFP levels on a Cell Lab Quanta SC flow cytometer (Beckman Coulter). Output GFP expression level distributions within the cell populations were measured using the following settings: 488 nm laser line, 525 nm bandpass filter, and a PMT setting of 5.83. Fluorescence data were collected from 10,000 viable cell counts of each culture sample under low flow rates. A non-induced cell population was used to set a background level, and cells exhibiting fluorescence above this background level are defined as the GFP-expressing cell population.

### *4.4.4. Characterization of device higher-order information processing properties*

Device responses are reported as output swings, or dynamic ranges of gene expression, in fluorescence units of expression in the presence of both inputs relative to the levels in the absence of inputs. To better represent the functional behaviors of the NOR and NAND operators, the output swings are reported as levels in the absence of inputs relative to the levels in the presence of both inputs. Output swings represent arithmetic differences between the expression levels in the absence and presence of appropriate molecular inputs. As previously described, 1 unit expression is defined as the gene expression level of the construct carrying the parental active ribozyme sTRSV relative to the background fluorescence level[24]. The expression level of the sTRSV construct is ~2% of that of the construct carrying the inactive ribozyme control sTRSV Contl or the full transcriptional range of 50 units of expression. Percent device response represents the expression level of an RNA device in the absence or presence of appropriate molecular inputs normalized to the expression level of the inactive ribozyme control sTRSV Contl.

Cooperative binding activities of RNA devices were determined using the Hill equation: $y = y_{\max} x^{n_H} / \left( x^{n_H} + K^{n_H} \right)$ where y is the gene expression response at an input concentration x, $y_{max}$ is the maximum gene expression response or saturation level, and $n_H$ and K represent the Hill coefficient and the ligand concentration at the half maximal response, respectively. Experiments demonstrate that the device responses begin to saturate at 10 mM theophylline, such that Hill coefficients were determined by normalizing dynamic switching ranges or device output swings between the absence and presence of 10 mM theophylline to 0-100% and plotting log [fraction expressed (or repressed) / (1 - fraction expressed (or repressed))] versus log [input concentration], where the slope represents the

Hill coefficient ($n_H$). All fluorescence data and mean ±s.d. are reported from at least three independent experiments.

## 4.5. Supplementary Information

**Supplementary Text 4.1:** *RNA device response properties and standards in data presentation*

There has been significant effort directed to the characterization of natural and engineered RNA devices. These efforts have resulted in important descriptions and demonstrations of RNA devices; however, the work is often reported through different metrics and standards. Standard means of reporting the characterized device properties are needed to accurately evaluate, compare, and appreciate the functional properties of the diverse RNA devices that have been developed or will be developed.

The RNA device properties that characterize the performance of a device include output swing (absolute difference of the dynamic range; here reported as device response), output fold induction or repression (ratio of the dynamic range: [signal in the presence (absence) of input]/[signal in the absence (presence) of input]), baseline expression (expression level in the absence of ligand; here reported as output basal signal), and input swing (input concentration over which device output changes). In order to fully characterize the dynamic range of an RNA device, either the baseline expression and the output swing or the baseline expression and the output fold induction (repression) should be reported. However, such dynamic range data cannot be compared across different genetic constructs and systems which can alter the observed response of an RNA device. For example, different organisms will have different transcriptional capacities; different regulated genes will have

different fold expression/activity levels (e.g., enzyme-based reporters exhibit turnover of a substrate and an amplified fold induction range relative to fluorescent protein-based reporters); and different promoters will have different fold transcriptional ranges. Therefore, reporting device response properties relative to standards are critical to enabling comparison of the performance of different devices within the context of different genetic constructs and systems.

Here, we propose the use of two standards in RNA device characterization: (i) the level of gene expression from the genetic construct (including promoter, gene, etc.) in the absence of the RNA device (100%; signal standard), and (ii) the level of gene expression in the absence of the genetic construct (0%; background standard). The proposed standards allow researchers to determine the performance of the RNA device across the full transcriptional range of a specified promoter, without any non-specific effects that an inactive RNA device might exhibit due to its location relative to other components in the genetic construct and its secondary structure. The use of reference standards is important because the RNA device (and therefore its performance) is coupled to other components in the genetic construct, including a promoter. Therefore, components can be changed to alter the baseline expression level relative to the signal standard as appropriate for a given application.

A device architecture that enables modification of baseline expression levels of single-input gates is shown in Figure 4.2A, where multiple single-input gate devices are coupled to alter both the baseline expression and output swing. We selected single-input gates with varying baseline expression levels to demonstrate the effects of gate coupling on baseline expression from the device (Figure 4.2B; Supplementary Text 4.2). We have

previously reported on a tuning strategy targeted to the transmitter component that can be used to build single-input gates with lower baseline expression levels (L2Bulge8; ~12%)[24]. Therefore, the combination of these two strategies (transmitter tuning and gate coupling) results in devices that exhibit much lower baseline expression levels (2xL2Bulge8; ~7%). We report output swing and baseline expression in Figure 4.2B to demonstrate the tuning of baseline expression. To simplify data presentation and focus on the response of the RNA devices to inputs, we report only output swing for most of the other devices in the main figures, and report baseline expression levels in the Supplementary Information (Supplementary Table 4.1). In addition, another straightforward way to alter the baseline expression from an RNA device is to alter the promoter that it is coupled to. For example, in the systems reported here all devices are coupled to a very strong promoter (GAL1-10). If we replaced that promoter with a weaker promoter, the baseline expression level would be much lower relative to the signal standard.

With the goal of integrating RNA devices into different genetic circuits (comprised of various biological components), such standardized characterization information is critical to match properties of the components in the circuit to achieve the desired system response. RNA devices do not necessarily need to exhibit output swings that span the full transcriptional range of a very strong promoter in order to be biologically relevant. Many endogenous proteins and enzymes are expressed at levels much lower than that obtained from the stronger promoters commonly used in recombinant work. In addition, proteins can exhibit very different thresholds of titratable function depending on their activities, such that a very low baseline expression level is not always necessary. Even natural riboswitches may not be used to titrate enzyme concentrations across their full response curves, as that would

require cells to regulate input metabolite concentrations to these regulators over a ~$10^4$-$10^5$-fold range. As such, an important property of RNA devices is their ability to be tuned to exhibit different device response properties using (1) energetic tuning strategies targeted to the transmitter component[24]; (2) coupled single-input gates (Figure 4.2B); and (3) component matching[36, 37]. These strategies provide important flexibility in tuning RNA device response to fit applications with different performance requirements. We have demonstrated previously that the output swings and baseline expression levels exhibited by RNA devices are biologically relevant, specifically in the application of intracellular detection of metabolic concentrations (where an output swing outside the noise in gene expression is important) and the regulation of cell growth/death (where the ability to titrate the output swing across a threshold concentration of the regulated protein is important)[24]. In addition, there are many other examples where non-coding RNAs play key regulatory roles in controlling biological function without exhibiting regulatory ranges across the full transcriptional range of the promoter system of the genetic construct[38-41].

**Supplementary Text 4.2:** *Predicted and observed response properties of coupled single-input gates*

Coupled single-input gate devices (SI 1) are comprised of single-input gates that are expected to act independently. Independent function of the single-input gates results in several predictions, regarding the response properties of such coupled gate devices relative to the single-input gates, previously described by Welz and Breaker in a tandem riboswitch system composed of two independent riboswitches[26]. However, the predicted changes in the

device response properties were not shown to be exhibited by the naturally-occurring functional counterpart[26], and are examined here for the synthetic devices.

The first predicted property of a coupled single-input gate device is that it will exhibit decreased basal output signals from the single-input gate. The expected decrease in basal output signal can be predicted from the single-input gate responses and follows a straightforward probability determination that both gates are in the ribozyme-inactive state (requiring AND behavior):

$$p_d = p_1 * p_2$$

where p is the fraction in the ribozyme-inactive state (determined as the percent gene expression relative to the ribozyme-inactive control); subscripts 1, 2, and d indicate single-input gate 1, single-input gate 2, and the coupled single-input gate device, respectively. The predicted and measured basal output signals are shown in Supplementary Table 4.1. For most of the coupled single-input gate devices the predicted and measured basal output signals match well, supporting the independent function of the single-input gates. There are two coupled single-input gate devices, both comprised of L2cm4, for which there is not a strong match between the predicted and measured values. The results indicate that L2cm4 may not function independently when coupled in a higher-order device. L2cm4 has a transmitter component that functions through a different mechanism than the other single-input gates examined here[24], specifically through a helix-slipping mechanism[42]. This information transmission mechanism requires the presence of non-Watson-Crick base pairs within the transmitter component, which may result in weaker device structural stability, potentially allowing non-specific interactions with surrounding sequences and thus interfering with the independent function of this single-input gate.

The effect of decreased basal output signal, has also been predicted to result in an increased dynamic range for such systems[26]. This would generally be true under situations in which the input concentration is saturating to the response of the system and irreversible rates do not dominate reversible rates. In the experimental systems examined here, the input ligands may not be at fully saturating concentrations due to transport limitations across the cell membrane and toxicity of the input molecules at high concentrations. In addition, in certain systems the irreversible rate of ribozyme cleavage may compete with the reversible rate of conformational switching.

The second and third predicted properties of coupled single-input gate devices apply to devices that respond to the same inputs (SI 1.1) and apply to the characteristics of the input-response curve. The second property is associated with the sensitivity of the device to input concentration. As previously pointed out, devices that couple Inverter gates (repress gene expression) are predicted to trigger a gene control response at lower input concentrations[26, 43]. This behavior results from such coupled Inverter gate devices functioning essentially through OR behavior, as the independent activation of either single-input gate device through input binding results in the repression of gene expression from a transcript. However, devices that couple Buffer gates (activate gene expression) are expected to trigger a gene control response at higher input concentrations, as the independent activation of both devices through input binding (AND behavior) is required to activate gene expression from a transcript.

The third property is associated with the slope of the response curve over ranges in gene expression. Coupled single-input gate devices are predicted to result in a more 'digital' response curve[26], where the same output dynamic range can be achieved with a lower change

in input concentration. This effect should be true for both coupled Inverter and Buffer gate devices, although the actual increase in the 'digital' nature of the response curve is predicted to be quite low[26]. In addition, this effect would only generally be true under situations in which the input concentration is saturating to the response of the system. For example, at lower input concentrations (i.e., input concentrations lower than the midway point of the input swing), the coupled Inverter gate device is predicted to have a higher slope than the single-input gate, whereas the coupled Buffer gate device is predicted to have a lower slope than the single-input gate. Therefore, the predicted effects on the slope of the response curve are anticipated to be small.

We measured the ligand response curves of two representative coupled single-input gate devices and their single-gate counterparts (Supplementary Text 4.2 Figure 1). The coupled Inverter gate device (2xL2bulgeOff1) exhibits a response at slightly lower concentrations of input than the single Inverter gate (L2bulgeOff1), whereas the coupled Buffer gate device (2xL2bulge1) exhibits a response at slightly higher concentrations of input than the single Buffer gate (L2bulge1). However, the observed changes in the response curves are very slight, such that strong conclusions on the effects of gate coupling on the input-response curves cannot be made.

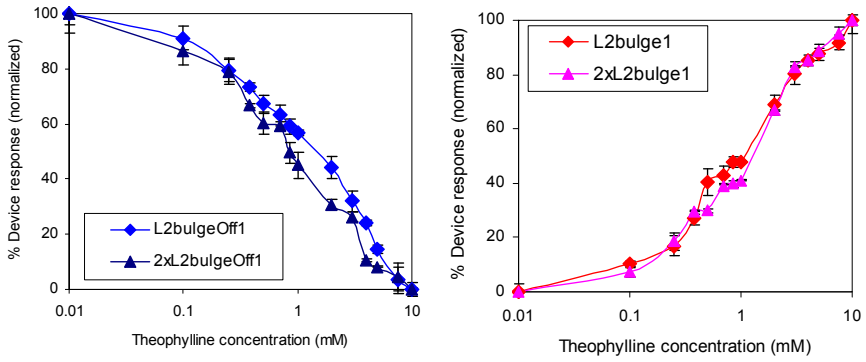


**Supplementary Text 4.2 Figure 1.** The device response over varying input concentrations of representative coupled gate devices (2xL2bulgeOff1, right; 2xL2bulge1, left) constructed

through SI 1.1 and their corresponding single-gate device counterparts (L2bulgeOff1, L2bulge1). The percent device response is plotted by normalizing corresponding dynamic switching ranges between the absence and presence of 10 mM theophylline to 0-100% as described in Materials and Methods.

**Supplementary Text 4.3:** *Layered architectures extend the information processing capabilities of SI 1*

The first assembly scheme based on signal integration within the 3' UTR provides modular composition frameworks for two basic logic operators, AND and NOR. Additional logic operators may be desired, including NAND and OR gates. One way in which to directly obtain these logic operations from the assembled operations in SI 1 is to invert the output from the AND and NOR gate operators, respectively (Supplementary Text 4.3 Figure 1). For example, the resulting output of the AND and NOR gates could be an Inverter device such as a repressor protein[20] or an inhibitory noncoding RNA[44] that acts on a separately encoded gene product resulting in the desired NAND and OR operations, respectively. However, this proposed framework results in a layered architecture, which may have less desirable properties such as loss of signal and longer signal processing times. Alternative assembly strategies for obtaining additional logic operations that result in non-layered architectures are described in the manuscript.

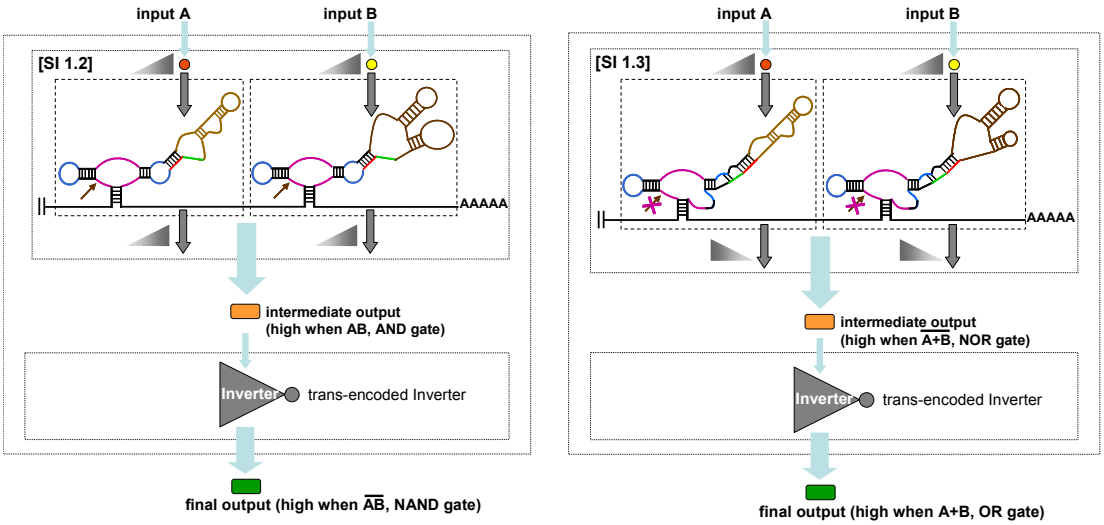

**Supplementary Text 4.3 Figure 1.** Schematic representation of layered architectures that extend the information processing capabilities of SI 1. Left, schematic illustrating a NAND gate operation by inverting the output of an AND gate. Right, schematic illustrating an OR gate operation by inverting the output of a NOR gate.

**Supplementary Text 4.4:** *Non-layered architectures (SI 2, SI 3) for an OR gate operation*

The second assembly scheme based on signal integration at the ribozyme core (SI 2) should be as flexible a composition framework as that specified for integration within the 3' UTR (SI 1). For example, SI 2 can be implemented to construct a higher-order RNA device capable of performing an OR gate operation by coupling internal Buffer gates responsive to different molecular inputs to stems I and II of the ribozyme (SI 2.2, Supplementary Text 4.4 Figure 1). While such a logic operation is theoretically possible, its construction is currently limited by the lack of one necessary component of this device - an internal Buffer gate coupled to stem I. Efforts are currently underway to generate such components. Therefore, SI 2 can provide logic operations that are not obtainable through SI 1 with non-layered architectures.

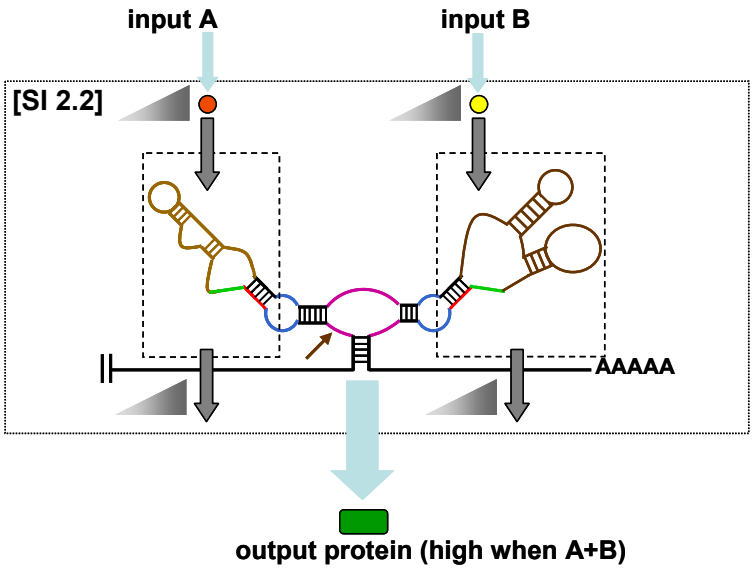


**Supplementary Text 4.4 Figure 1.** Schematic representation of an RNA device based on SI 2 that functions as an OR gate operator.

Alternatively, devices that perform an OR gate operation can be constructed through SI 3 (signal integration through a single ribozyme stem) by coupling a theophylline-responsive internal Buffer gate (IG1) and a tetracycline-responsive internal Inverter gate (IG2) at stem II (Supplementary Text 4.4 Figure 2A). The assembly scheme is similar to that used to construct devices that perform an AND gate operation, described in Figure 4.4A, except that the energetic requirements for switching between the conformational states are different. This RNA device (SI 3.3) assumes the conformation in which the binding pockets for both inputs are formed (Supplementary Text 4.4 Figure 2A) with a lower energetic requirement than an AND gate device ($\Delta\Delta G_{IG12}$ in SI 3.3 < $\Delta\Delta G_{IG2}$+ $\Delta\Delta G_{IG1}$ in SI 3.1), effectively allowing either input to bind to its corresponding sensor. The resulting device exhibits low output in the absence of both molecular inputs and high output in the presence of either input or both (Supplementary Text 4.4 Figure 2B). We constructed two OR gate devices, tc/theo-On1 and tc/theo-On2, based on different IG2 transmitter components.

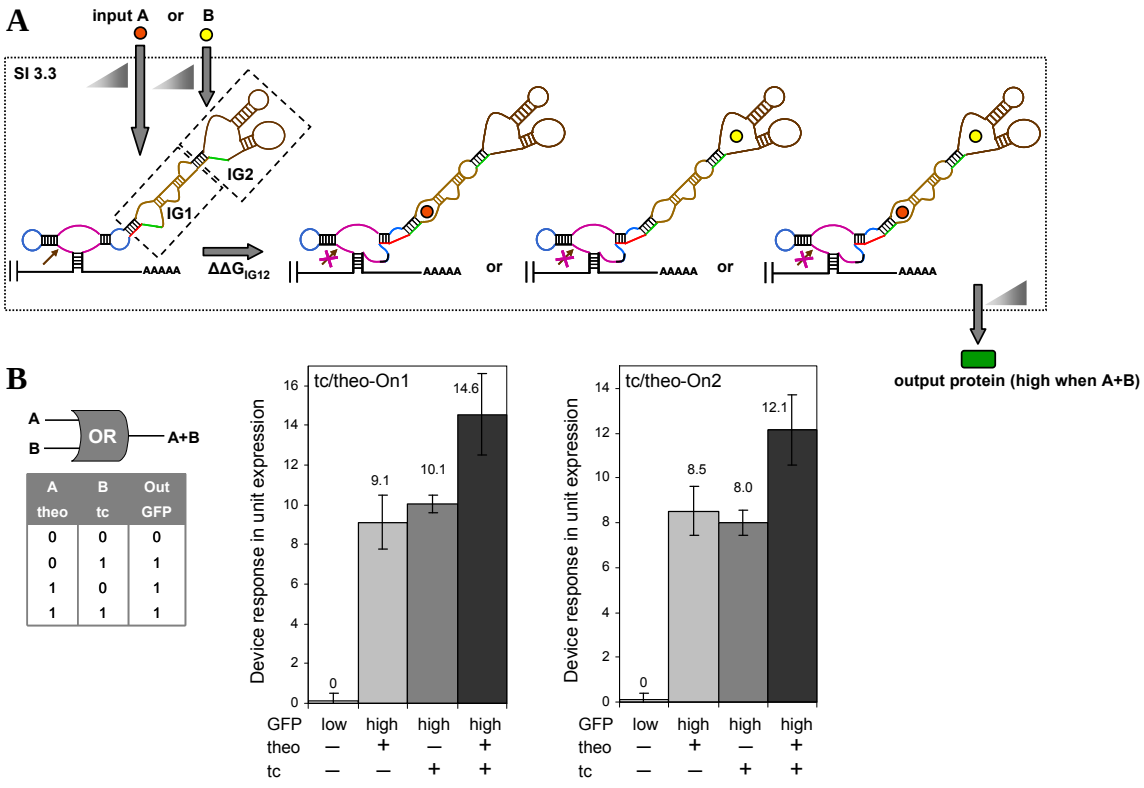

**Supplementary Text 4.4 Figure 2.** OR gate devices. (A) Schematic representation of an RNA device that performs an OR gate operation by coupling internal Buffer (IG1) and Inverter (IG2) gates responsive to different input molecules to a single ribozyme stem. (B) The device response and truth table of OR gate operators (tc/theo-On1 and tc/theo-On2) based on SI 3.3. Device response under different input conditions (theo or tc (-), 0 mM; theo (+), 10 mM; tc (+), 0.25 mM) is reported as the output swing in units of expression relative to the absence of both inputs as described in Materials and Methods.

**Supplementary Text 4.5:** *Programming signal gain through multiple sensor-transmitter components*

Cooperativity in biological molecules is often a result of multiple binding sites that transit from a low-affinity state to a high-affinity state as more ligands occupy the available binding sites. In RNA devices comprised of two internal gates to the same input, although the sensor components exhibit similar input affinities ($K_{apt}$), their effective affinities are a combined effect of the sensor affinity ($K_{apt}$) and the energetic requirements for the device to switch between two states ($K_{IG}$), the latter of which can be programmed into the transmitter component ($\Delta\Delta G_{IG}$). Thus, the difference in free energies between states 1 and 3 ($\Delta\Delta G_{IG2}$+ $\Delta\Delta G_{IG1}$) represents an energetic contribution which lowers the effective binding affinity of IG1 to its input. The difference in free energies between states 1 and 2 ($\Delta\Delta G_{IG2}$) represents a lower energetic contribution to the effective binding affinity of IG2 to its input, such that the effective binding affinity of IG2 is higher than that of IG1. However, binding of input to IG2 lowers the energetic contribution to IG1 to the difference in free energies between states 2 and 3 ($\Delta\Delta G_{IG1}$), resulting in an increase in effective binding affinity as a result of input binding to IG2. The RNA device design is expected to result in a larger change in the regulatory response as input concentrations increase and IG1 transits from a lower affinity state to a higher affinity state. By programming the energetic differences between the

different conformational states ($\Delta\Delta G_{IG2}$ and $\Delta\Delta G_{IG1}$), we can program the degree of cooperativity (or level of signal gain) exhibited by the system (Supplementary Table 4.2).

**Supplementary Text 4.6:** *Device sequences*

The sequences of all devices used in this work are described below. Color schemes in the sequences correspond to those in the schematic device diagrams: purple, catalytic core of the ribozyme or actuator component; blue, loop regions of the actuator component; brown, aptamer or sensor component; green and red, competing and switching strands of the transmitter component, respectively; orange, communication modules of the transmitter component; italicized, spacer sequences; underlined, restriction sites.

**Single-input gates**

**Single-input Buffer gates**

L2bugle1

5’CCTAGG*AAACAAACAAA*GCTGTCACCGGATGTGCTTTCCGGTCTGATGAGTCCGT

GTCCATACCAGCATCGTCTTGATGCCCTTGGCAGGGACGGGACGAGGACGAAAC

AGC*AAAAAGAAAAATAAAAA*CTCGAG

L2bulge5

5’CCTAGG*AAACAAACAAA*GCTGTCACCGGATGTGCTTTCCGGTCTGATGAGTCCGT

GTCCAATACCAGCATCGTCTTGATGCCCTTGGCAGTGGACGGGACGAGGACGAA

ACAGC*AAAAAGAAAAATAAAAA*CTCGAG

L2bulge9

5’CCTAGG*AAACAAACAAA*GCTGTCACCGGATGTGCTTTCCGGTCTGATGAGTCCGT

TGTCCAATACCAGCATCGTCTTGATGCCCTTGGCAGTGGATGGGGACGGAGGAC

GAAACAGC*AAAAAGAAAAATAAAAA*CTCGAG

L2bulge1tc

5’CCTAGG*AAACAAACAAA*GCTGTCACCGGATGTGCTTTCCGGTCTGATGAGTCCGT

GTCCAAAACATACCAGATTTCGATCTGGAGAGGTGAAGAATTCGACCACCTGGA

CGGGACGAGGACGAAACAGC*AAAAAGAAAAATAAAAA*CTCGAG

**Single-input Inverter gates**

L2bulgeOff1

5’CCTAGG*AAACAAACAAA*GCTGTCACCGGATGTGCTTTCCGGTCTGATGAGTCCGT

GTTGCTGATACCAGCATCGTCTTGATGCCCTTGGCAGCAGTGGACGAGGACGAA

ACAGC*AAAAAGAAAAATAAAAA*CTCGAG

L2bulgeOff1tc

5’CCTAGG*AAACAAACAAA*GCTGTCACCGGATGTGCTTTCCGGTCTGATGAGTCCGT

TGTTGAGGAAAACATACCAGATTTCGATCTGGAGAGGTGAAGAATTCGACCACC

TCCTTATGGGAGGACGAAACAGC*AAAAAGAAAAATAAAAA*CTCGAG

L2bulgeOff2tc

5’CCTAGG*AAACAAACAAA*GCTGTCACCGGATGTGCTTTCCGGTCTGATGAGTCCGT

ATGAGGAAAACATACCAGATTTCGATCTGGAGAGGTGAAGAATTCGACCACCTC

CTTAGAGGAGGACGAAACAGC*AAAAAGAAAAATAAAAA*CTCGAG

L2bulgeOff3tc

5’CCTAGG*AAACAAACAAA*GCTGTCACCGGATGTGCTTTCCGGTCTGATGAGTCCGT

TGATGAGGAAAACATACCAGATTTCGATCTGGAGAGGTGAAGAATTCGACCACC

TCCTTAGAGGAGGACGAAACAGC*AAAAAGAAAAATAAAAA*CTCGAG

L2cm4

5’CCTAGG*AAACAAACAAA*GCTGTCACCGGATGTGCTTTCCGGTCTGATGAGTCCGT

CCTGGATACCAGCATCGTCTTGATGCCCTTGGCAGTCATAGAGGACGAAACAGC

*AAAAAGAAAAATAAAAA*CTCGAG

L1cm10

5’CCTAGG*AAACAAACAAA*GCTGTCACCGGATGTAAATGATACCAGCATCGTCTTG

ATGCCCTTGGCAGCTGCGCTTTCCGGTCTGATGAGTCCGTGAGGACGAAACAGC*A*

*AAAAGAAAAATAAAAA*CTCGAG

**Higher-order devices (SI 1: signal integration within the 3’ UTR)**

**Two coupled Buffer or Inverter gates responsive to the same input**

2xL2bulge1

5’CCTAGG*AAACAAACAAA*GCTGTCACCGGATGTGCTTTCCGGTCTGATGAGTCCGT

GTCCATACCAGCATCGTCTTGATGCCCTTGGCAGGGACGGGACGAGGACGAAAC

AGCAAAAAGAAAAATAAAAACTCGAGAAACAAACAAAGCTGTCACCGGATGTG

CTTTCCGGTCTGATGAGTCCGTGTCCATACCAGCATCGTCTTGATGCCCTTGGCA

GGGACGGGACGAGGACGAAACAGC*AAAAAGAAAAATAAAAA*CTCGAG

2xL2bulgeOff1

5’CCTAGG*AAACAAACAAA*GCTGTCACCGGATGTGCTTTCCGGTCTGATGAGTCCGT

GTTGCTGATACCAGCATCGTCTTGATGCCCTTGGCAGCAGTGGACGAGGACGAA

ACAGCAAAAAGAAAAATAAAAACTCGAGAAACAAACAAAGCTGTCACCGGATG

TGCTTTCCGGTCTGATGAGTCCGTGTTGCTGATACCAGCATCGTCTTGATGCCCTT

GGCAGCAGTGGACGAGGACGAAACAGC*AAAAAGAAAAATAAAAA*CTCGAG

Note: The sequence assembly of other RNA devices based on SI 1 (2xL2bulge1tc, 2xL2cm4, (L2bulge1+L2bulge9), and (L2bulgeOff1+L2cm4)), and the bandpass filter operator (L2bulge1+L2bulgeOff1) is identical to that of 2xL2bulge1 or 2xL2bulgeOff1, illustrated above as example templates. Sequences of single-input gates are shown above.

**AND gates**

AND1 (L2bulge1+L2bulge1tc)

5’CCTAGG*AAACAAACAAA*GCTGTCACCGGATGTGCTTTCCGGTCTGATGAGTCCGT

GTCCATACCAGCATCGTCTTGATGCCCTTGGCAGGGACGGGACGAGGACGAAAC

AGCAAAAAGAAAAATAAAAACTCGAGAAACAAACAAAGCTGTCACCGGATGTG

CTTTCCGGTCTGATGAGTCCGTGTCCAAAACATACCAGATTTCGATCTGGAGAGG

TGAAGAATTCGACCACCTGGACGGGACGAGGACGAAACAGC*AAAAAGAAAAATAA*

*AAA*CTCGAG

AND2 (L2bulge9+L2bulge1tc)

5’CCTAGG*AAACAAACAAA*GCTGTCACCGGATGTGCTTTCCGGTCTGATGAGTCCGT

TGTCCAATACCAGCATCGTCTTGATGCCCTTGGCAGTGGATGGGGACGGAGGAC

GAAACAGCAAAAAGAAAAATAAAAACTCGAGAAACAAACAAAGCTGTCACCGG

ATGTGCTTTCCGGTCTGATGAGTCCGTGTCCAAAACATACCAGATTTCGATCTGG

AGAGGTGAAGAATTCGACCACCTGGACGGGACGAGGACGAAACAGC*AAAAAGAA*

*AAATAAAAA*CTCGAG

**NOR gates**

NOR1 (L2bulgeOff1+L2bulgeOff1tc)

5’CCTAGG*AAACAAACAAA*GCTGTCACCGGATGTGCTTTCCGGTCTGATGAGTCCGT

GTTGCTGATACCAGCATCGTCTTGATGCCCTTGGCAGCAGTGGACGAGGACGAA

ACAGCAAAAAGAAAAATAAAAACTCGAGAAACAAACAAAGCTGTCACCGGATG

TGCTTTCCGGTCTGATGAGTCCGTTGTTGAGGAAAACATACCAGATTTCGATCTG

GAGAGGTGAAGAATTCGACCACCTCCTTATGGGAGGACGAAACAGC*AAAAAGAAA*

*AATAAAAA*CTCGAG

NOR2 (L2bulgeOff1+L2bulgeOff2tc)

5’CCTAGG*AAACAAACAAA*GCTGTCACCGGATGTGCTTTCCGGTCTGATGAGTCCGT

GTTGCTGATACCAGCATCGTCTTGATGCCCTTGGCAGCAGTGGACGAGGACGAA

ACAGCAAAAAGAAAAATAAAAACTCGAGAAACAAACAAAGCTGTCACCGGATG

TGCTTTCCGGTCTGATGAGTCCGTATGAGGAAAACATACCAGATTTCGATCTGGA

GAGGTGAAGAATTCGACCACCTCCTTAGAGGAGGACGAAACAGC*AAAAAGAAAAA*

*TAAAAA*CTCGAG

**Higher-order devices (SI 2: signal integration at the ribozyme core through two stems)**

**NAND gates**

NAND1 (L1cm10-L2bulgeOff1tc)

5’CCTAGG*AAACAAACAAA*GCTGTCACCGGATGTAAATGATACCAGCATCGTCTTG

ATGCCCTTGGCAGCTGCGCTTTCCGGTCTGATGAGTCCGTTGTTGAGGAAAACAT

ACCAGATTTCGATCTGGAGAGGTGAAGAATTCGACCACCTCCTTATGGGAGGAC

GAAACAGC*AAAAAGAAAAATAAAAA*CTCGAG

NAND2 (L1cm10-L2bulgeOff3tc)

5’CCTAGG*AAACAAACAAA*GCTGTCACCGGATGTAAATGATACCAGCATCGTCTTG

ATGCCCTTGGCAGCTGCGCTTTCCGGTCTGATGAGTCCGTTGATGAGGAAAACAT

ACCAGATTTCGATCTGGAGAGGTGAAGAATTCGACCACCTCCTTAGAGGAGGAC

GAAACAGC*AAAAAGAAAAATAAAAA*CTCGAG

**Higher-order devices (SI 3: signal integration at a single ribozyme stem)**

**AND gates**

AND1 (tc-theo-On1)

5’CCTAGG*AAACAAACAAA*GCTGTCACCGGATGTGCTTTCCGGTCTGATGAGTCCGT

GTCCATACCAGCATCGCTCAAAACATACCAGATTTCGATCTGGAGAGGTGAAGA

ATTCGACCACCTGAGTCTTGATGCCCTTGGCAGGGACGGGACGAGGACGAAACA

GC*AAAAAGAAAAATAAAAA*CTCGAG

AND2 (tc-theo-On2)

5’CCTAGG*AAACAAACAAA*GCTGTCACCGGATGTGCTTTCCGGTCTGATGAGTCCGT

GTCCATACCAGCATCGCTAAAACATACCAGATTTCGATCTGGAGAGGTGAAGAA

TTCGACCACCTAGTCTTGATGCCCTTGGCAGGGACGGGACGAGGACGAAACAGC

*AAAAAGAAAAATAAAAA*CTCGAG

AND3 (tc-theo-On3)

5’CCTAGG*AAACAAACAAA*GCTGTCACCGGATGTGCTTTCCGGTCTGATGAGTCCGT

GTCCATACCAGCATCGTGTAAAACATACCAGATTTCGATCTGGAGAGGTGAAGA

ATTCGACCACCTACATCTTGATGCCCTTGGCAGGGACGGGACGAGGACGAAACA

GC*AAAAAGAAAAATAAAAA*CTCGAG

**OR gates**

OR1 (tc/theo-On1)

5’CCTAGG*AAACAAACAAA*GCTGTCACCGGATGTGCTTTCCGGTCTGATGAGTCCGT

GTCCATACCAGCATCGGGCCTAAAACATACCAGATTTCGATCTGGAGAGGTGAA

GAATTCGACCACCTAGGTTTCTTGATGCCCTTGGCAGGGACGGGACGAGGACGA

AACAGC*AAAAAGAAAAATAAAAA*CTCGAG

OR2 (tc/theo-On2)

5’CCTAGG*AAACAAACAAA*GCTGTCACCGGATGTGCTTTCCGGTCTGATGAGTCCGT

GTCCATACCAGCATCGGTGGTAAAACATACCAGATTTCGATCTGGAGAGGTGAA

GAATTCGACCACCTACCATTCTTGATGCCCTTGGCAGGGACGGGACGAGGACGA

AACAGC*AAAAAGAAAAATAAAAA*CTCGAG

**Two coupled internal gates responsive to the same input**

theo-theo-On1

5’CCTAGG*AAACAAACAAA*GCTGTCACCGGATGTGCTTTCCGGTCTGATGAGTCCGT

GTCCATACCAGCATCGTTTATACCAGCATCGTCTTGATGCCCTTGGCAGAAATCT

TGATGCCCTTGGCAGGGACGGGACGAGGACGAAACAGC*AAAAAGAAAAATAAAAA*

CTCGAG

theo-theo-On2

5’CCTAGG*AAACAAACAAA*GCTGTCACCGGATGTGCTTTCCGGTCTGATGAGTCCGT

GTCCATACCAGCATCGTTGAATACCAGCATCGTCTTGATGCCCTTGGCAGTTGAT

CTTGATGCCCTTGGCAGGGACGGGACGAGGACGAAACAGC*AAAAAGAAAAATAAA*

*AA*CTCGAG

theo-theo-On3

5’CCTAGG*AAACAAACAAA*GCTGTCACCGGATGTGCTTTCCGGTCTGATGAGTCCGT

GTCCATACCAGCATCGATTGATACCAGCATCGTCTTGATGCCCTTGGCAGCAGTT

CTTGATGCCCTTGGCAGGGACGGGACGAGGACGAAACAGC*AAAAAGAAAAATAAA*

*AA*CTCGAG

theo-theo-On4

5’CCTAGG*AAACAAACAAA*GCTGTCACCGGATGTGCTTTCCGGTCTGATGAGTCCGT

GTCCATACCAGCATCGTATGATACCAGCATCGTCTTGATGCCCTTGGCAGCGTAT

CTTGATGCCCTTGGCAGGGACGGGACGAGGACGAAACAGC*AAAAAGAAAAATAAA*

*AA*CTCGAG

theo-theo-On5

5’CCTAGG*AAACAAACAAA*GCTGTCACCGGATGTGCTTTCCGGTCTGATGAGTCCGT

GTCCATACCAGCATCGATCATACCAGCATCGTCTTGATGCCCTTGGCAGGATTCT

TGATGCCCTTGGCAGGGACGGGACGAGGACGAAACAGC*AAAAAGAAAAATAAAAA*

CTCGAG

theo-theo-On6

5’CCTAGG*AAACAAACAAA*GCTGTCACCGGATGTGCTTTCCGGTCTGATGAGTCCGT

GTCCATACCAGCATCGATTGATACCAGCATCGTCTTGATGCCCTTGGCAGCAATT

CTTGATGCCCTTGGCAGGGACGGGACGAGGACGAAACAGC*AAAAAGAAAAATAAA*

*AA*CTCGAG

theo-theo-On7

5’CCTAGG*AAACAAACAAA*GCTGTCACCGGATGTGCTTTCCGGTCTGATGAGTCCGT

GTCCATACCAGCATCGGTAAATACCAGCATCGTCTTGATGCCCTTGGCAGTTGCT

CTTGATGCCCTTGGCAGGGACGGGACGAGGACGAAACAGC*AAAAAGAAAAATAAA*

*AA*CTCGAG

theo-theo-On8

5’CCTAGG*AAACAAACAAA*GCTGTCACCGGATGTGCTTTCCGGTCTGATGAGTCCGT

GTCCATACCAGCATCGTTGAATACCAGCATCGTCTTGATGCCCTTGGCAGTTGAT

CTTGATGCCCTTGGCAGGGACGGGACGAGGACGAAACAGC*AAAAAGAAAAATAAA*

*AA*CTCGAG

theo-theo-On9

5’CCTAGG*AAACAAACAAA*GCTGTCACCGGATGTGCTTTCCGGTCTGATGAGTCCGT

GTCCATACCAGCATCGGTTGAATACCAGCATCGTCTTGATGCCCTTGGCAGTTGA

TTCTTGATGCCCTTGGCAGGGACGGGACGAGGACGAAACAGC*AAAAAGAAAAATA*

*AAAA*CTCGAG

theo-theo-On10 (Cooperative Buffer gate)

5’CCTAGG*AAACAAACAAA*GCTGTCACCGGATGTGCTTTCCGGTCTGATGAGTCCGT

GTCCATACCAGCATCGGTTGAATACCAGCATCGTCTTGATGCCCTTGGCAGTTGA

CTCTTGATGCCCTTGGCAGGGATAGGACGAGGACGAAACAGC*AAAAAGAAAAATA*

*AAAA*CTCGAG

theo-theo-On11 (Cooperative Buffer gate)

5’CCTAGG*AAACAAACAAA*GCTGTCACCGGATGTGCTTTCCGGTCTGATGAGTCCGT

GTCCATACCAGCATCGGTTGAATACCAGCATCGTCTTGATGCCCTTGGCAGTTGA

TTCTTGATGCCCTTGGCAGGGATAGGACGAGGACGAAACAGC*AAAAAGAAAAATA*

*AAAA*CTCGAG

theo-theo-On12 (Cooperative Buffer gate)

5’CCTAGG*AAACAAACAAA*GCTGTCACCGGATGTGCTTTCCGGTCTGATGAGTCCGT

GTCCATACCAGCATCGATTGAATACCAGCATCGTCTTGATGCCCTTGGCAGTTGA

TTCTTGATGCCCTTGGCAGGGATAGGACGAGGACGAAACAGC*AAAAAGAAAAATA*

*AAAA*CTCGAG

theo-theo-On13 (Cooperative Buffer gate)

5’CCTAGG*AAACAAACAAA*GCTGTCACCGGATGTGCTTTCCGGTCTGATGAGTCCGT

GTCCATACCAGCATCGTGTTATACCAGCATCGTCTTGATGCCCTTGGCAGAATGT

CTTGATGCCCTTGGCAGGGATAGGACGAGGACGAAACAGC*AAAAAGAAAAATAAA*

*AA*CTCGAG

**Two coupled internal Inverter gates responsive to the same input**

theo-theo-Off1

5’CCTAGG*AAACAAACAAA*GCTGTCACCGGATGTGCTTTCCGGTCTGATGAGTCCGT

GTTATGATACCAGCATCGACATACCAGCATCGTCTTGATGCCCTTGGCAGGTTCT

TGATGCCCTTGGCAGCATGGACGAGGACGAAACAGC*AAAAAGAAAAATAAAAA*CTC

GAG

theo-theo-Off2

5’CCTAGG*AAACAAACAAA*GCTGTCACCGGATGTGCTTTCCGGTCTGATGAGTCCGT

GTTGCTGATACCAGCATCGACATACCAGCATCGTCTTGATGCCCTTGGCAGGTTC

TTGATGCCCTTGGCAGCAGTGGACGAGGACGAAACAGC*AAAAAGAAAAATAAAAA*C

TCGAG

theo-theo-Off3

5’CCTAGG*AAACAAACAAA*GCTGTCACCGGATGTGCTTTCCGGTCTGATGAGTCCGT

GTTATGATACCAGCATCGGACATACCAGCATCGTCTTGATGCCCTTGGCAGGTTT

CTTGATGCCCTTGGCAGCATGGACGAGGACGAAACAGC*AAAAAGAAAAATAAAAA*C

TCGAG

theo-theo-Off4

5’CCTAGG*AAACAAACAAA*GCTGTCACCGGATGTGCTTTCCGGTCTGATGAGTCCGT

GTGTCTGATACCAGCATCGACATACCAGCATCGTCTTGATGCCCTTGGCAGGTTC

TTGATGCCCTTGGCAGCAGGGACGAGGACGAAACAGC*AAAAAGAAAAATAAAAA*CT

CGAG

theo-theo-Off5

5’CCTAGG*AAACAAACAAA*GCTGTCACCGGATGTGCTTTCCGGTCTGATGAGTCCGT

GTGTCCTGATACCAGCATCGGACATACCAGCATCGTCTTGATGCCCTTGGCAGGT

TTCTTGATGCCCTTGGCAGCAGGGACGAGGACGAAACAGC*AAAAAGAAAAATAAAA*

*A*CTCGAG

theo-theo-Off6 (Cooperative Inverter gate)

5’CCTAGG*AAACAAACAAA*GCTGTCACCGGATGTGCTTTCCGGTCTGATGAGTCCGT

GTTATGATACCAGCATCGGCATACCAGCATCGTCTTGATGCCCTTGGCAGGTTCT

TGATGCCCTTGGCAGCATGGACGAGGACGAAACAGC*AAAAAGAAAAATAAAAA*CTC

GAG

theo-theo-Off7

5’CCTAGG*AAACAAACAAA*GCTGTCACCGGATGTGCTTTCCGGTCTGATGAGTCCGT

GTTGCTGATACCAGCATCGACATACCAGCATCGTCTTGATGCCCTTGGCAGGTTC

TTGATGCCCTTGGCAGCAGGGACGAGGACGAAACAGC*AAAAAGAAAAATAAAAA*CT

CGAG

theo-theo-Off8

5’CCTAGG*AAACAAACAAA*GCTGTCACCGGATGTGCTTTCCGGTCTGATGAGTCCGT

GTGTTTGATACCAGCATCGACATACCAGCATCGTCTTGATGCCCTTGGCAGGTTC

TTGATGCCCTTGGCAGCAAGGACGAGGACGAAACAGC*AAAAAGAAAAATAAAAA*CT

CGAG

**Mutated coupled internal gates**

theo-theo-On1M1

5’CCTAGG*AAACAAACAAA*GCTGTCACCGGATGTGCTTTCCGGTCTGATGAGTCCGT

GTCCAGACCAGCATCGTTTATACCAGCATCGTCTTGATGCCCTTGGCAGAAATCT

TGATGCCTATGGCAGGGACGGGACGAGGACGAAACAGC*AAAAAGAAAAATAAAAA*

CTCGAG

theo-theo-On1M2

5’CCTAGG*AAACAAACAAA*GCTGTCACCGGATGTGCTTTCCGGTCTGATGAGTCCGT

GTCCATACCAGCATCGTTTATACCAGCATCGTCTTGATGCCTATGGCAGAAATCT

TGATGCCCTTGGCAGGGACGGGACGAGGACGAAACAGC*AAAAAGAAAAATAAAAA*

CTCGAG

theo-theo-On13M1

5’CCTAGG*AAACAAACAAA*GCTGTCACCGGATGTGCTTTCCGGTCTGATGAGTCCGT

GTCCATACCAGCATCGTGTTATACCAGCATCGTCTTGATGCCCTTGGCAGAATGT

CTTGATGCCTATGGCAGGGATAGGACGAGGACGAAACAGC*AAAAAGAAAAATAAA*

*AA*CTCGAG

theo-theo-On13M2

5’CCTAGG*AAACAAACAAA*GCTGTCACCGGATGTGCTTTCCGGTCTGATGAGTCCGT

GTCCATACCAGCATCGTGTTAGACCAGCATCGTCTTGATGCCTATGGCAGAATGT

CTTGATGCCCTTGGCAGGGATAGGACGAGGACGAAACAGC*AAAAAGAAAAATAAA*

*AA*CTCGAG

theo-theo-Off2M1

5’CCTAGG*AAACAAACAAA*GCTGTCACCGGATGTGCTTTCCGGTCTGATGAGTCCGT

GTTGCTGAGACCAGCATCGACATACCAGCATCGTCTTGATGCCCTTGGCAGGTTC

TTGATGCCTATGGCAGCAGTGGACGAGGACGAAACAGC*AAAAAGAAAAATAAAAA*C

TCGAG

theo-theo-Off2M2

5’CCTAGG*AAACAAACAAA*GCTGTCACCGGATGTGCTTTCCGGTCTGATGAGTCCGT

GTTGCTGATACCAGCATCGACATACCAGCATCGTCTTGATGCCTATGGCAGGTTC

TTGATGCCCTTGGCAGCAGTGGACGAGGACGAAACAGC*AAAAAGAAAAATAAAAA*C

TCGAG

theo-theo-Off6M1

5’CCTAGG*AAACAAACAAA*GCTGTCACCGGATGTGCTTTCCGGTCTGATGAGTCCGT

GTTATGAACCCAGCATCGGCATACCAGCATCGTCTTGATGCCCTTGGCAGGTTCT

TGATGCCTATGGCAGCATGGACGAGGACGAAACAGC*AAAAAGAAAAATAAAAA*CTC

GAG

theo-theo-Off6M2

5’CCTAGG*AAACAAACAAA*GCTGTCACCGGATGTGCTTTCCGGTCTGATGAGTCCGT

GTTATGATACCAGCATCGGCATACCAGCATCGTCTTGATGCCTATGGCAGGTTCT

TGATGCCCTTGGCAGCATGGACGAGGACGAAACAGC*AAAAAGAAAAAT*AAAAACTC

GAG

**Supplementary Figures**

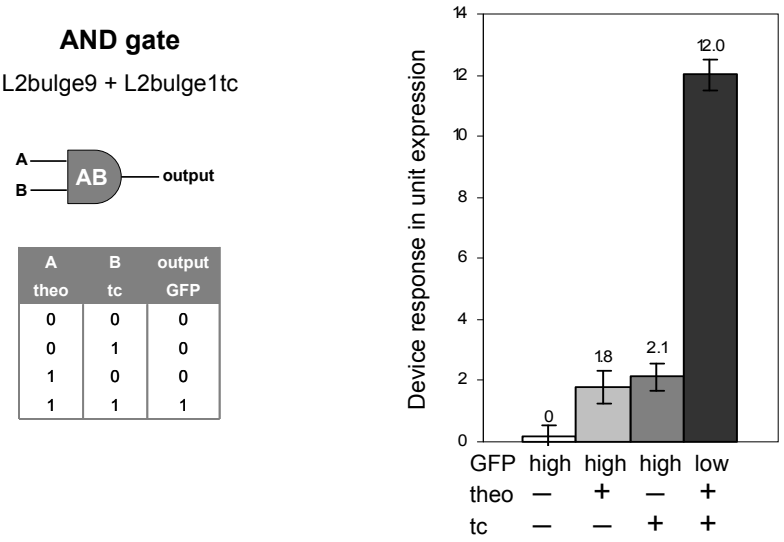


**Supplementary Figure 4.1.** The device response and truth table of an AND gate operator (L2bulge9+L2bulge1tc) based on SI 1.2. The RNA device is constructed by coupling a theophylline-responsive Buffer gate (L2bulge9) and a tetracycline-responsive Buffer gate (L2bulge1tc) in the 3’ UTR of a target transcript. Device response under different input conditions (theo or tc (-), 0 mM; theo (+), 5 mM; tc (+), 0.5 mM) is reported as the output swing in units of expression relative to the absence of both inputs as described in Materials and Methods.

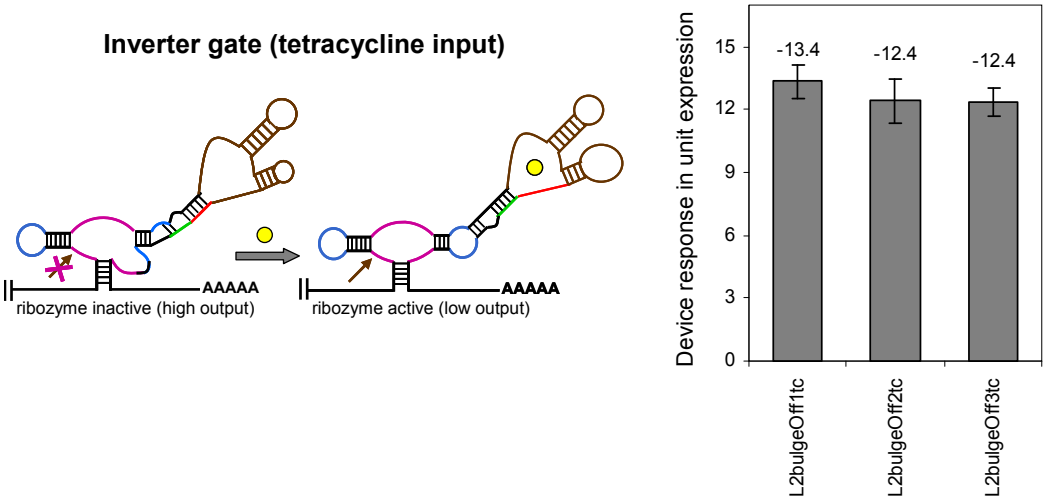


**Supplementary Figure 4.2.** Schematic representation and device response of tetracycline-responsive Inverter gates. Color schemes follow those described in Figure 4.1. Device response is reported as the output swing in units of expression as described in Materials and Methods. Output swings are reported from 0 mM to 0.5 mM tetracycline. The negative sign indicates the down-regulation of target gene expression by Inverter gates.

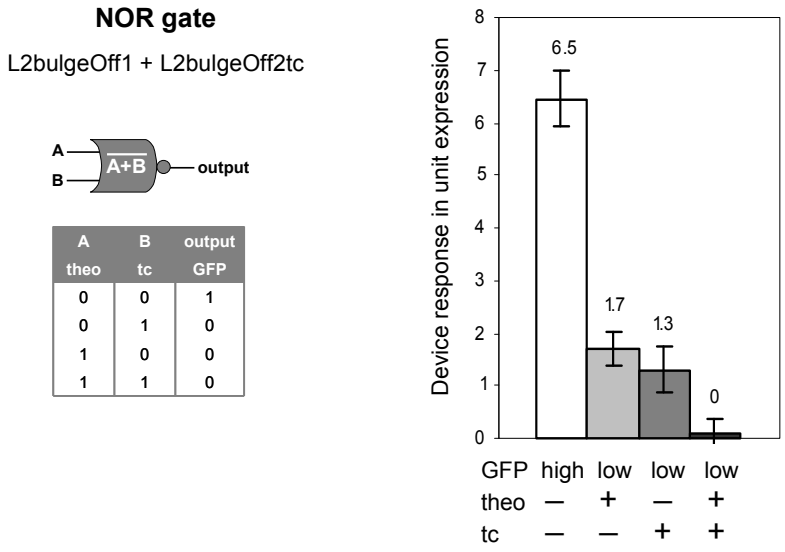


| A | B | output |
|---|---|---|
| theo | tc | GFP |
| 0 | 0 | 1 |
| 0 | 1 | 0 |
| 1 | 0 | 0 |
| 1 | 1 | 0 |

**Supplementary Figure 4.3.** The device response and truth table of a NOR gate operator (L2bulgeOff1+L2bulgeOff2tc) based on SI 1.3. The RNA device is constructed by coupling a theophylline-responsive Inverter gate (L2bulgeOff1) and a tetracycline-responsive Inverter gate (L2bulgeOff2tc) in the 3' UTR of a target transcript. Device response under different input conditions (theo or tc (-), 0 mM; theo (+), 10 mM; tc (+), 0.5 mM) is reported as the output swing in units of expression relative to the presence of both inputs as described in Materials and Methods.

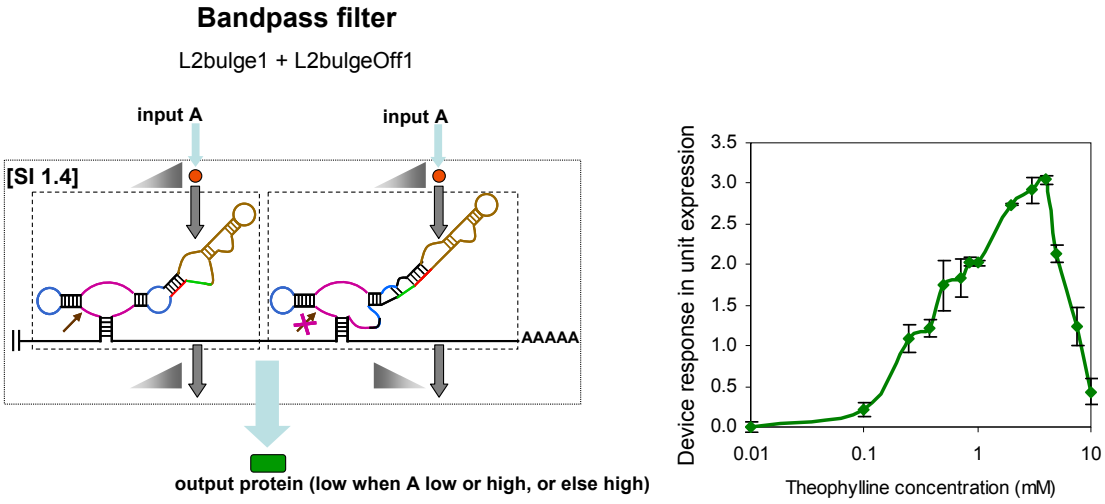


**Supplementary Figure 4.4.** Schematic representation and device response of a bandpass filter operator (L2bulge1+L2bulgeOff1) based on SI 1.4. Color schemes follow those described in Figure 4.1. Each gate is indicated in a boxed region, and triangles indicate relationships between associated gate inputs and outputs. The RNA device is constructed by coupling a theophylline-responsive Buffer gate (L2bulge1) and a theophylline-responsive Inverter gate (L2bulgeOff1) in the 3' UTR of a target transcript. Device response is reported as the output swing in units of expression as a function of theophylline concentration relative to the absence of theophylline as described in Materials and Methods.

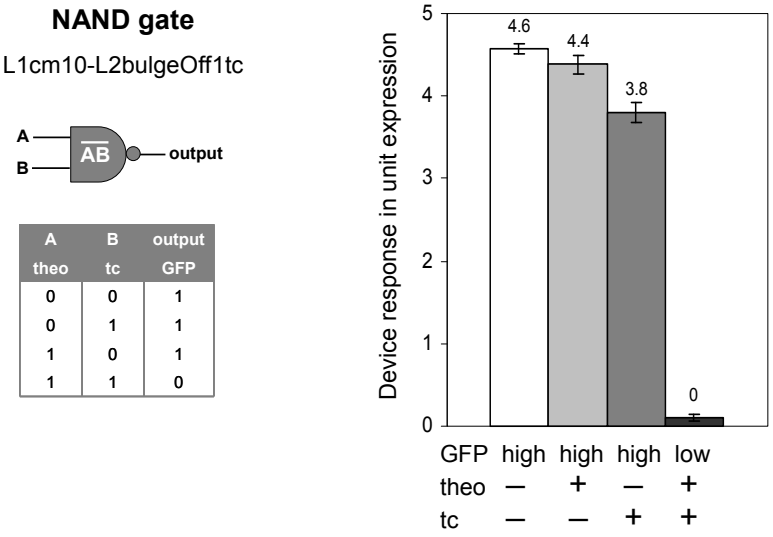


| A theo | B tc | output GFP |
|---|---|---|
| 0 | 0 | 1 |
| 0 | 1 | 1 |
| 1 | 0 | 1 |
| 1 | 1 | 0 |

**Supplementary Figure 4.5.** The device response and truth table of a NAND gate operator (L1cm10-L2bulgeOff1tc) based on SI 2.1. The RNA device is constructed by coupling a theophylline-responsive internal Inverter gate (L1cm10) and a tetracycline-responsive internal Inverter gate (L2bulgeOff1tc) to stems I and II, respectively, of a ribozyme. Device response under different input conditions (theo or tc (-), 0 mM; theo (+), 10 mM; tc (+), 1 mM) is reported as the output swing in units of expression relative to the presence of both inputs as described in Materials and Methods.

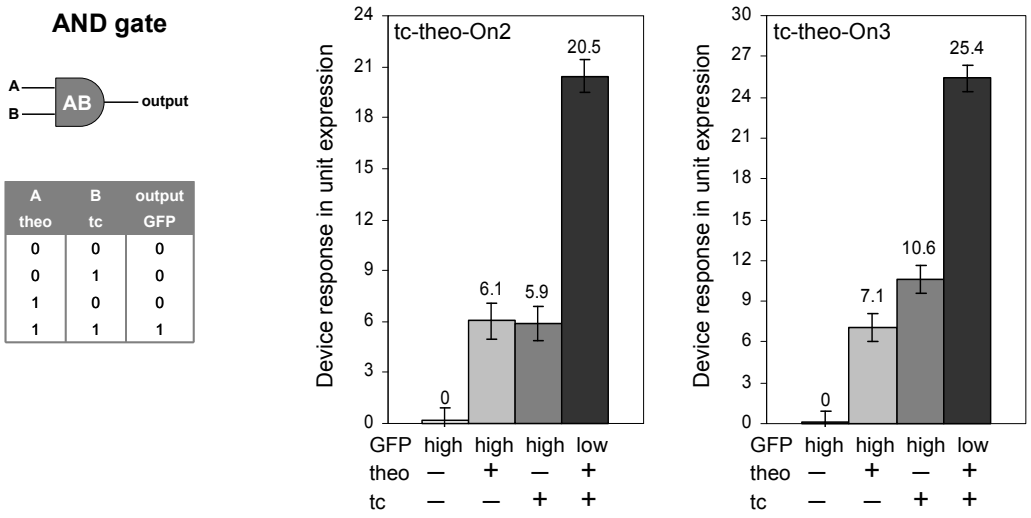


**Supplementary Figure 4.6.** The device response and truth table of AND gate operators (tc-theo-On2 and tc-theo-On3) based on SI 3.1. The RNA devices are constructed by coupling a theophylline-responsive internal Buffer gate (IG1) and a tetracycline-responsive internal Inverter gate (IG2) to stem II of a ribozyme. Device response under different input conditions (theo or tc (-), 0 mM; theo (+), 2.5 mM; tc (+), 0.5 mM) is reported as the output swing in units of expression relative to the absence of both inputs as described in Materials and Methods.

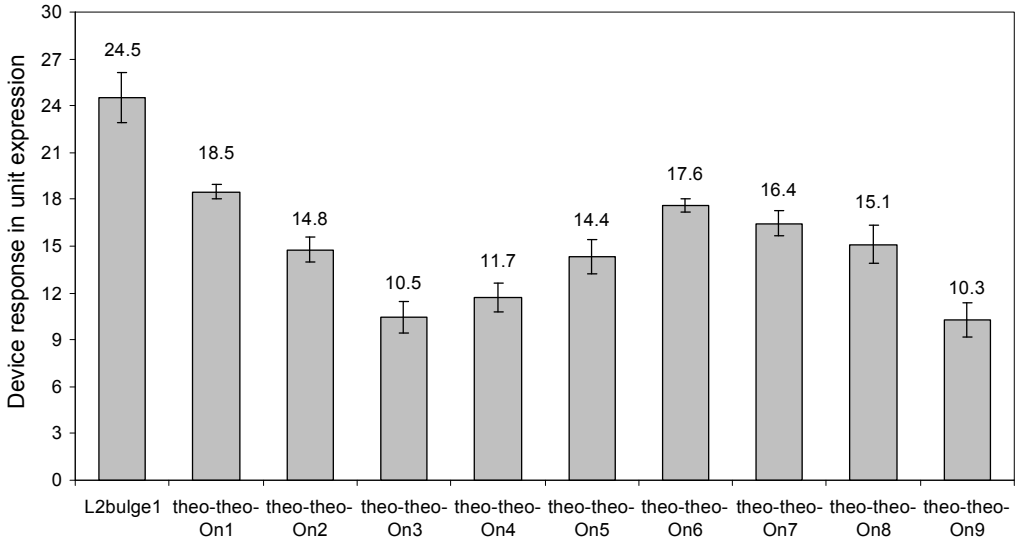


**Supplementary Figure 4.7.** The device response of RNA devices comprised of internal Buffer and Inverter gates and their single internal gate device counterpart (L2bulge1). The RNA devices are constructed by coupling theophylline-responsive internal Buffer (IG1) and Inverter (IG2) gates to stem II of a ribozyme. Device response is reported as the output swing in units of expression as described in Materials and Methods. Output swings are reported from 0 mM to 10 mM theophylline.

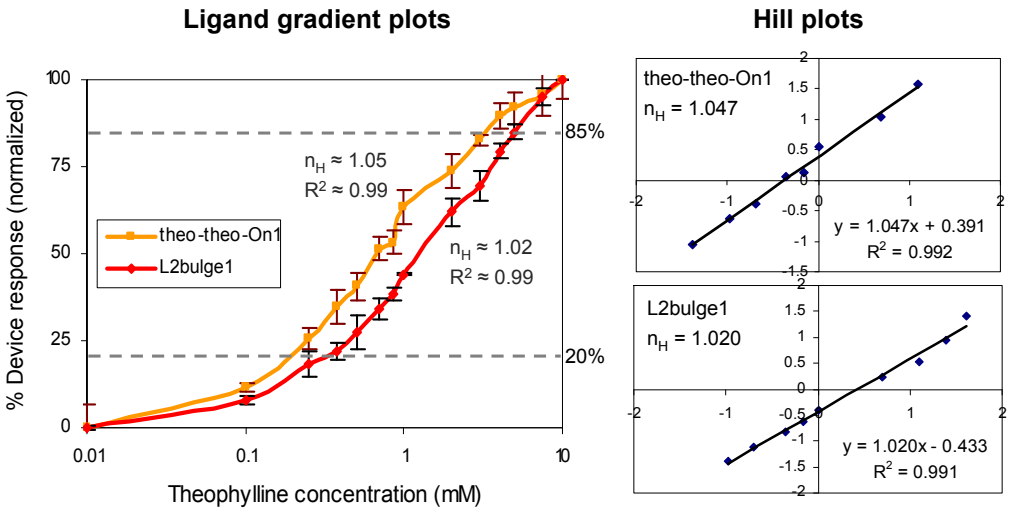


**Supplementary Figure 4.8.** The device response over varying input concentrations of a representative RNA device comprised of internal Buffer and Inverter gates (theo-theo-On1) and its single internal gate device counterpart (L2bulge1) demonstrates no signal gain ($n_H \approx 1$). The percent device response is plotted by normalizing corresponding dynamic switching ranges between the absence and presence of 10 mM theophylline to 0-100% as described in Materials and Methods. Corresponding Hill plots are constructed for 20-85% of each device switching range by plotting log [fraction expressed / (1 - fraction expressed)] against log [input concentration], where the slope represents the Hill coefficient ($n_H$).

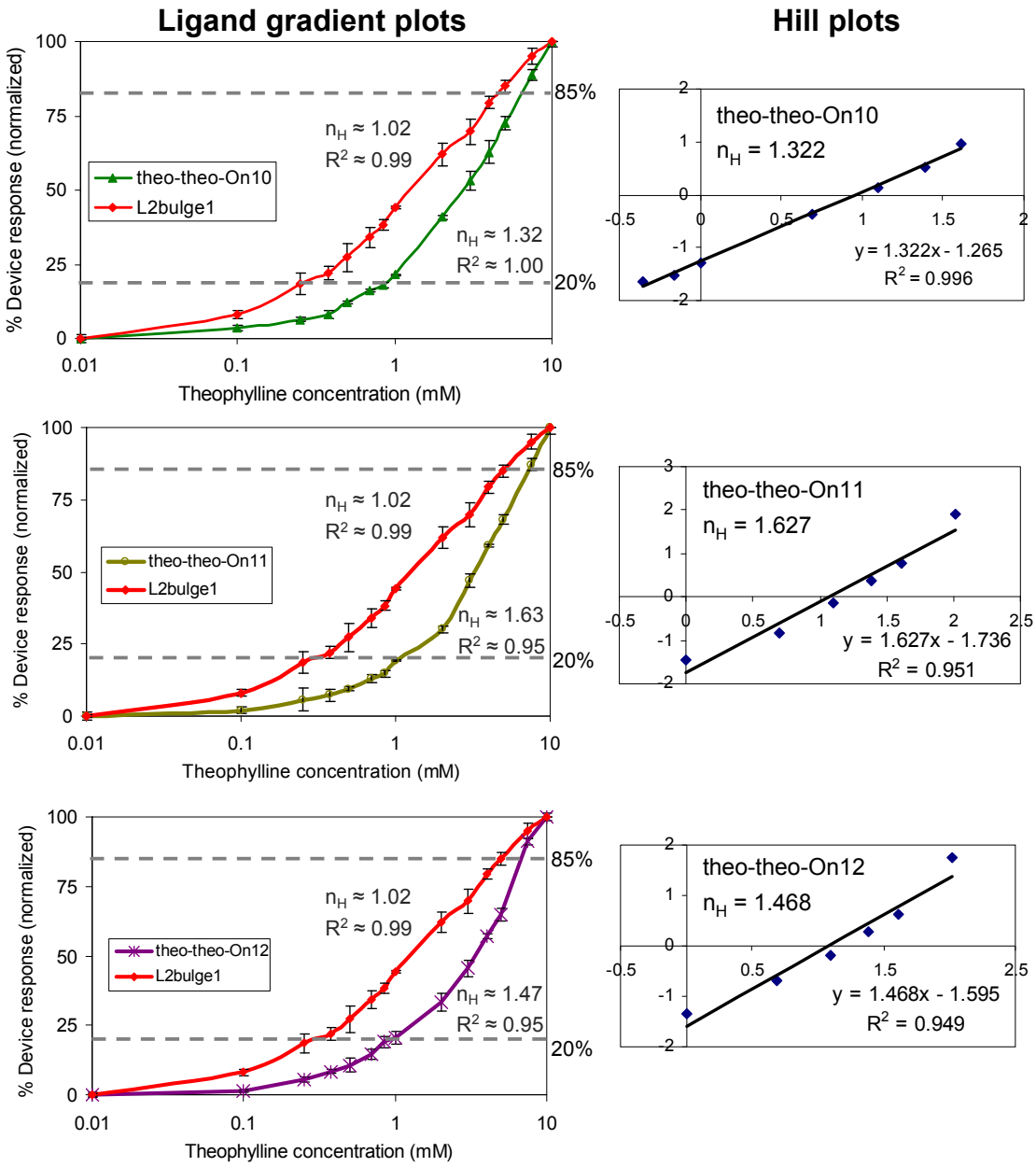


**Supplementary Figure 4.9.** The device response over varying input concentrations of RNA devices comprised of internal Buffer and Inverter gates (theo-theo-On10–12) and their single internal gate device counterpart (L2bulge1) demonstrates programmed cooperativity. The percent device response is plotted by normalizing corresponding dynamic switching ranges between the absence and presence of 10 mM theophylline to 0-100% as described in Materials and Methods. Corresponding Hill plots are constructed for 20-85% of each device switching range by plotting log [fraction expressed / (1 - fraction expressed)] against log [input concentration], where the slope represents the Hill coefficient ($n_H$).

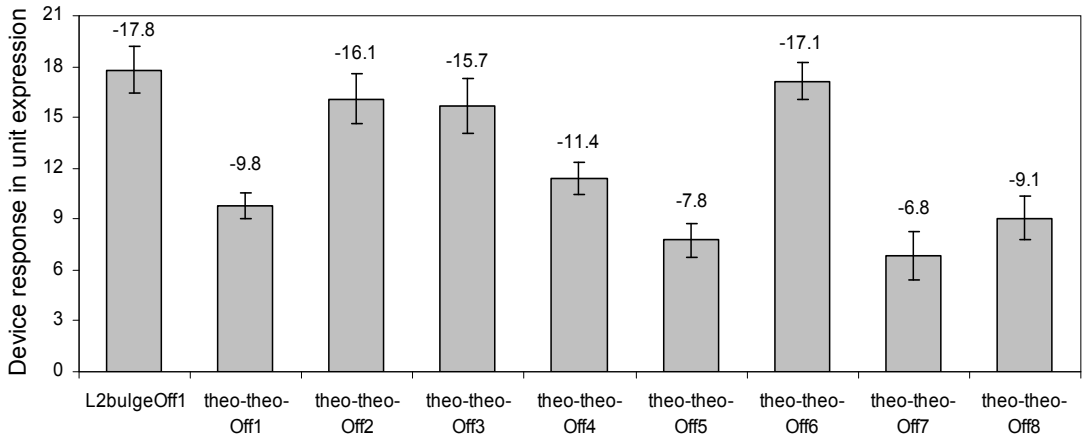


**Supplementary Figure 4.10.** The device response of RNA devices comprised of two internal Inverter gates and their single internal gate device counterpart (L2bulgeOff1). The RNA devices are constructed by coupling two theophylline-responsive internal Inverter gates (IG1, IG2) to stem II of a ribozyme. Device response is reported as the output swing in units of expression as described in Materials and Methods. Output swings are reported from 0 mM to 10 mM theophylline. The negative sign indicates the down-regulation of target gene expression.

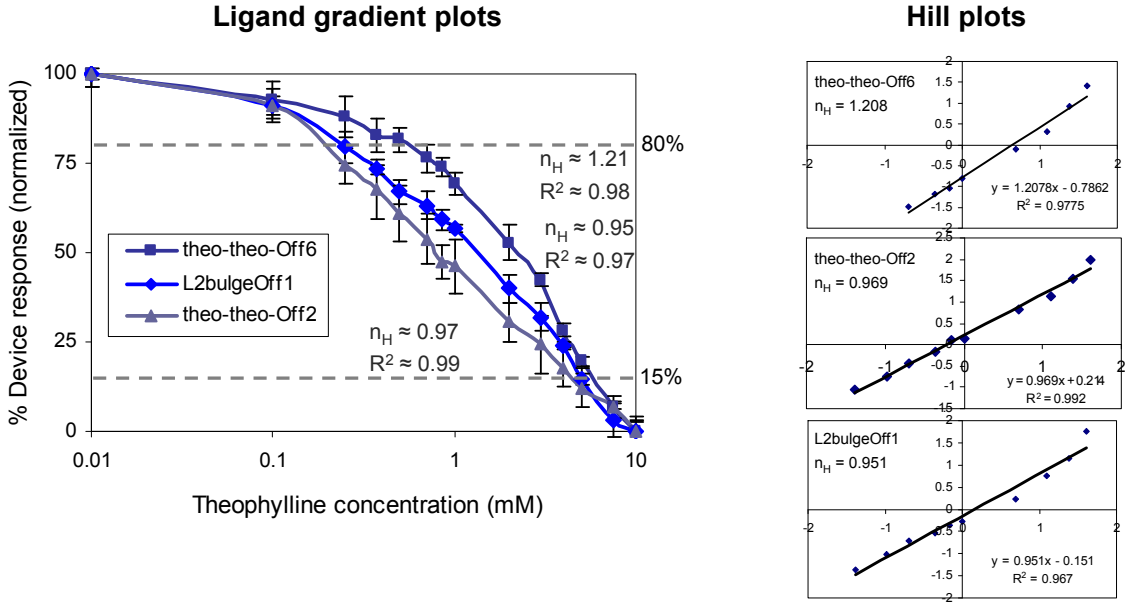


**Supplementary Figure 4.11.** The device response over varying theophylline concentrations of representative RNA devices comprised of two internal Inverter gates (theo-theo-Off2, $n_H \approx 1$; theo-theo-Off6, $n_H \approx 1.2$), and their single internal gate device counterpart (L2bulgeOff1, $n_H \approx 1$). The percent device response is plotted by normalizing corresponding dynamic switching ranges between the absence and presence of 10 mM theophylline to 0-100% as described in Materials and Methods. Corresponding Hill plots are constructed for 15-80% of each device switching range by plotting log [fraction repressed / (1 - fraction repressed)] against log [input concentration], where the slope represents the Hill coefficient ($n_H$).

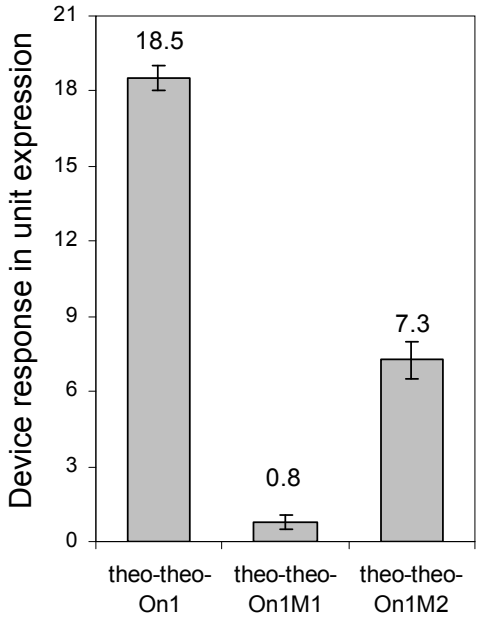


**Supplementary Figure 4.12.** The device response of a representative RNA device comprised of internal Buffer and Inverter gates (theo-theo-On1) and its mutated sensor variants demonstrates that input binding at both internal gates is responsible for the device response. Theo-theo-On1M1, mutation to the sensor in IG1; theo-theo-On1M2, mutation to sensor in IG2. Device response is reported as the output swing in units of expression as described in Materials and Methods. Output swings are reported from 0 mM to 10 mM theophylline. Individual mutations in both internal gates exhibited considerably lower output levels, supporting that both internal gates contribute to the overall device response. However, it was observed that theo-theo-On1M2 demonstrated less inhibition of device response compared to theo-theo-On1M1. The mutation of IG1 is anticipated to have a more significant impact on device performance as the device response is directly regulated by IG1.

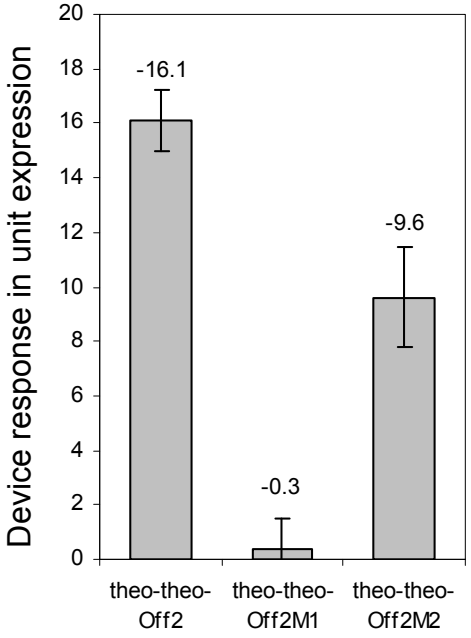


**Supplementary Figure 4.13.** The device response of a representative RNA device comprised of two internal Inverter gates (theo-theo-Off2) and its mutated sensor variants demonstrates that input binding at both internal gates is responsible for the device response. Theo-theo-Off2M1, mutation to the sensor in IG1; theo-theo-Off2M2, mutation to sensor in IG2. Device response is reported as the output swing in units of expression as described in Materials and Methods. Output swings are reported from 0 mM to 10 mM theophylline. The negative sign indicates the down-regulation of target gene expression. The mutation of IG1 is anticipated to have a more significant impact on device performance as the device response is directly regulated by IG1.

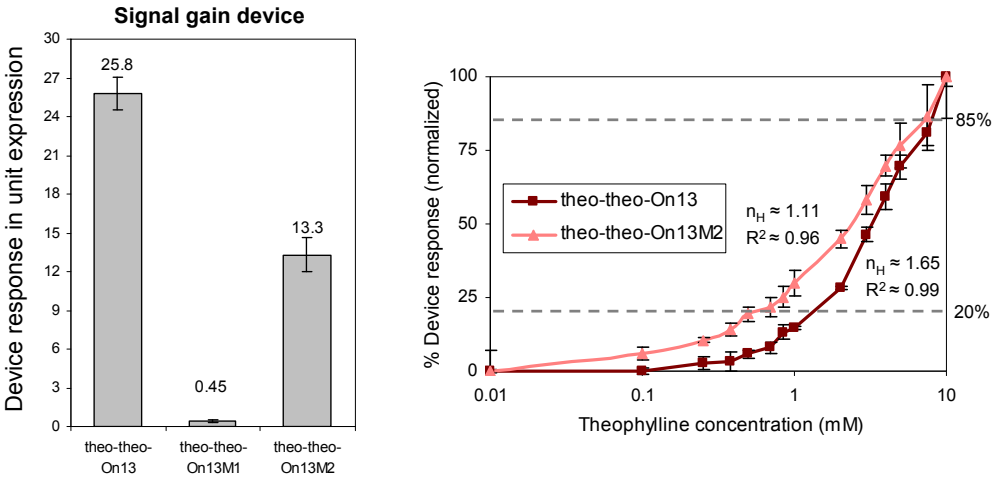


**Supplementary Figure 4.14.** The device response of a representative RNA device comprised of internal Buffer and Inverter gates that exhibits programmed cooperativity (theo-theo-On13) and its mutated sensor variants demonstrates that input binding at both internal gates is responsible for the device response. Theo-theo-On13M1, mutation to the sensor in IG1; theo-theo-On13M2, mutation to sensor in IG2. Device response is reported as the output swing in units of expression as described in Materials and Methods. Output swings are reported from 0 mM to 10 mM theophylline. The percent device response is plotted as described in Figure. 4.4E. The mutation of IG1 is anticipated to have a more significant impact on device performance as the device response is directly regulated by IG1.

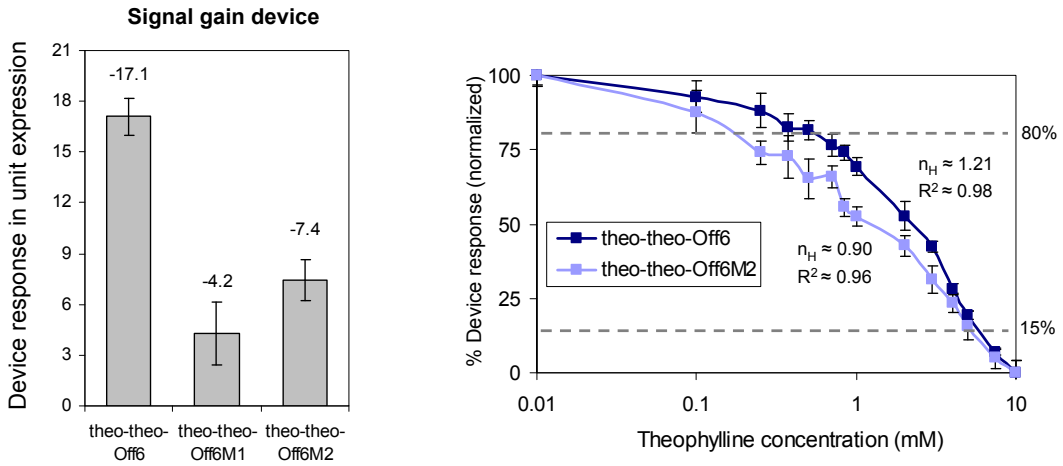


**Supplementary Figure 4.15.** The device response of a representative RNA device comprised of two internal Inverter gates that exhibits programmed cooperativity (theo-theo-Off6) and its mutated sensor variants demonstrates that input binding at both internal gates is responsible for the device response. Theo-theo-Off6M1, mutation to the sensor in IG1; theo-theo-Off6M2, mutation to sensor in IG2. Device response is reported as the output swing in units of expression as described in Materials and Methods. Output swings are reported from 0 mM to 10 mM theophylline. The negative sign indicates the down-regulation of target gene expression. The percent device response is plotted as described in Materials and Methods. The mutation of IG1 is anticipated to have a more significant impact on device performance as the device response is directly regulated by IG1.

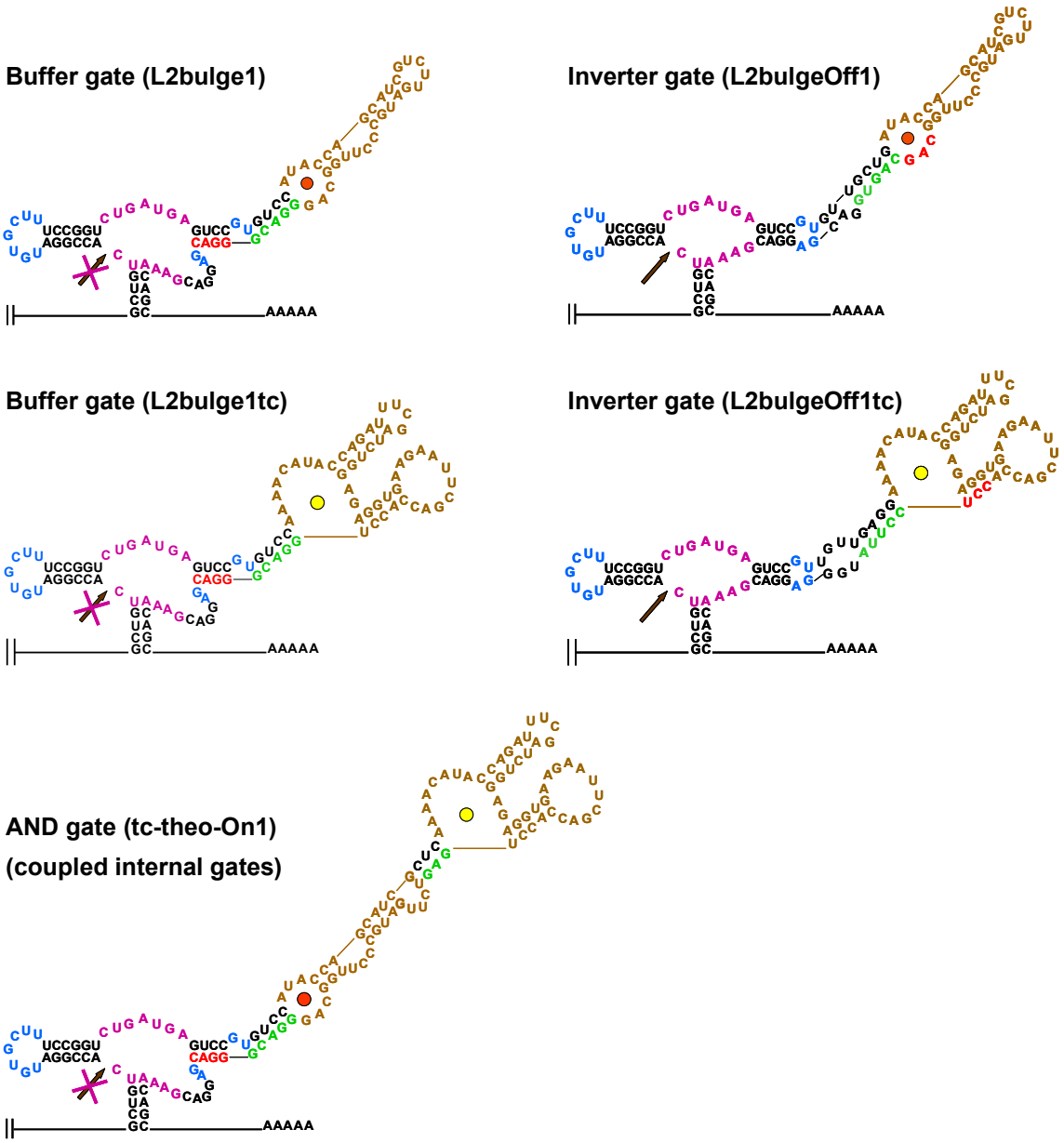


**Supplementary Figure 4.16.** Secondary structures and sequences of input-bound states of representative RNA devices. Single-input Buffer gates: L2bulge1, L2bulge1tc; single-input Inverter gates: L2bulgeOff1, L2bulgeOff1tc; RNA device comprised of internal Buffer (IG1) and Inverter (IG2) gates responsive to different inputs, illustrating points of coupling of two sensor-transmitter components: tc-theo-On1.

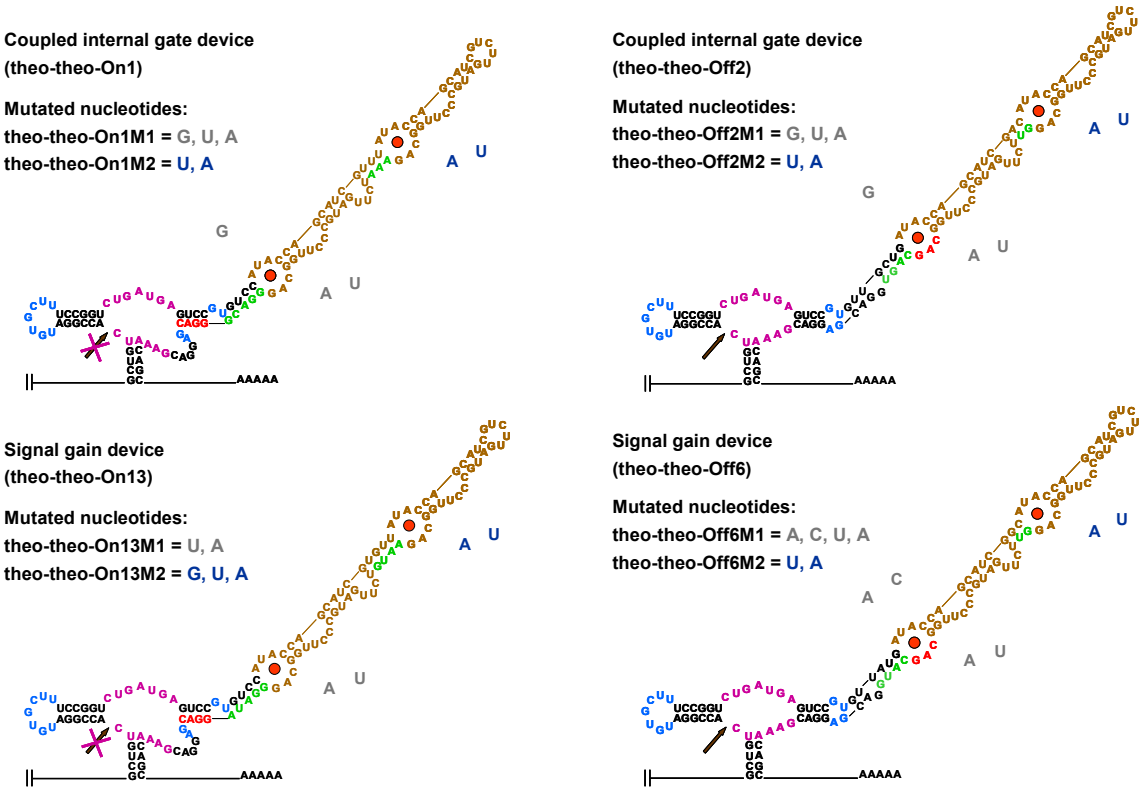


**Supplementary Figure 4.17.** Secondary structures and sequences of input-bound states of representative RNA device comprised of internal Buffer and Inverter gates responsive to the same input, illustrating points of coupling of two sensor-transmitter components. Nucleotides that were altered in the mutational studies are indicated for the sensors in IG1 and IG2. RNA devices that do not exhibit programmed cooperativity: theo-theo-On1, theo-theo-Off2; RNA devices that exhibit programmed cooperativity: theo-theo-On13, theo-theo-Off6.

**Supplementary Table 4.1.** The basal output signals and output swings of the RNA devices studied in this work are shown in % device response over the full transcriptional range of the employed promoter. The predicted basal output signals of coupled devices based on the appropriate single-gate response(s) and independent function are also reported. Predicted signals that do not match the measured output signals are indicated in italics.

| Device | % Device response (over the full transcriptional range) | | | | predicted basal signal for coupled devices |
|---|---|---|---|---|---|
| | theo, tc (-) | theo (+) | tc (+) | theo, tc (+) | |
| **SI 1.1** | | | | | |
| L2bulge1tc (Buffer) | 0.37 | | 0.96 | | |
| 2xL2bulge1tc (Buffer) | 0.16 | | 0.46 | | 0.14 |
| L2bulge1 (Buffer) | 0.40 | 0.89 | | | |
| 2xL2bulge1 (Buffer) | 0.20 | 0.37 | | | 0.16 |
| L2bugle8 (Buffer) | 0.12 | 0.48 | | | |
| 2xL2bulge8 (Buffer) | 0.07 | 0.19 | | | 0.01 |
| L2bulge5 (Buffer) | 0.82 | 1.00 | | | |
| L2bulge1+L2bulge5 (Buffer) | 0.25 | 0.43 | | | 0.33 |
| L2bulgeOff1 (Inverter) | 0.62 | 0.26 | | | |
| 2xL2bulgeOff1 (Inverter) | 0.37 | 0.21 | | | 0.38 |
| L2cm4 (Inverter) | 0.78 | 0.41 | | | |
| 2xL2cm4 (Inverter) | 0.32 | 0.20 | | | *0.61* |
| L2bulgeOff1+L2cm4 (Inverter) | 0.31 | 0.17 | | | *0.48* |
| | | | | | |
| **tc-responsive Inverter gates** | | | | | |
| L2bulgeOff1tc (Inverter) | 0.39 | | 0.12 | | |
| L2bulgeOff2tc (Inverter) | 0.42 | | 0.17 | | |
| L2bulgeOff3tc (Inverter) | 0.42 | | 0.17 | | |
| | | | | | |
| **SI 1.2 (AND gate)** | | | | | |
| L2bulge1+L2bulge1tc | 0.18 | 0.22 | 0.24 | 0.46 | 0.15 |
| L2bulge9+L2bulge1tc | 0.12 | 0.15 | 0.16 | 0.36 | 0.11 |
| L2bulge9 (single-input Buffer) | 0.30 | 0.72 | | | |
| | | | | | |
| **SI 1.3 (NOR gate)** | | | | | |
| L2bulgeOff1+L2bulgeOff1tc | 0.27 | 0.15 | 0.13 | 0.11 | 0.24 |
| L2bulgeOff1+L2bulgeOff2tc | 0.28 | 0.18 | 0.17 | 0.15 | 0.26 |
| | | | | | |
| **SI 2.1 (NAND gate)** | | | | | |
| L1cm10+L2bulgeOff3tc | 0.54 | 0.52 | 0.55 | 0.43 | |
| L1cm10+L2bulgeOff1tc | 0.51 | 0.51 | 0.50 | 0.42 | |
| | | | | | |
| **SI 3.1 (AND gate)** | | | | | |
| tc-theo-On1 | 0.36 | 0.48 | 0.50 | 0.89 | |
| tc-theo-On2 | 0.39 | 0.51 | 0.51 | 0.80 | |
| tc-theo-On3 | 0.39 | 0.53 | 0.61 | 0.90 | |
| | | | | | |
| **SI 3.2 (dual sensor-transmitter)** | | | | | |
| **Buffer function** | | | | | |
| theo-theo-On1 | 0.36 | 0.73 | | | |
| theo-theo-On2 | 0.41 | 0.70 | | | |
| theo-theo-On3 | 0.54 | 0.75 | | | |
| theo-theo-On4 | 0.66 | 0.89 | | | |
| theo-theo-On5 | 0.69 | 0.98 | | | |
| theo-theo-On6 | 0.46 | 0.81 | | | |
| theo-theo-On7 | 0.42 | 0.75 | | | |
| theo-theo-On8 | 0.31 | 0.61 | | | |
| theo-theo-On9 | 0.23 | 0.44 | | | |
| theo-theo-On10 (cooperative) | 0.16 | 0.54 | | | |
| theo-theo-On11 (cooperative) | 0.13 | 0.55 | | | |
| theo-theo-On12 (cooperative) | 0.12 | 0.60 | | | |
| theo-theo-On13 (cooperative) | 0.23 | 0.75 | | | |
| **Inverter function** | | | | | |
| theo-theo-Off1 | 0.34 | 0.15 | | | |
| theo-theo-Off2 | 0.60 | 0.27 | | | |
| theo-theo-Off3 | 0.67 | 0.36 | | | |
| theo-theo-Off4 | 0.47 | 0.24 | | | |
| theo-theo-Off5 | 0.40 | 0.24 | | | |
| theo-theo-Off6 (cooperative) | 0.58 | 0.24 | | | |
| theo-theo-Off7 | 0.54 | 0.40 | | | |
| theo-theo-Off8 | 0.43 | 0.24 | | | |
| | | | | | |
| **SI 3.3 (OR gate)** | | | | | |
| tc/theo-On1 | 0.48 | 0.65 | 0.64 | 0.72 | |
| tc/theo-On2 | 0.42 | 0.60 | 0.62 | 0.71 | |

**Supplementary Table 4.2.** Free energy changes associated with RNA devices comprised of internal Buffer and Inverter gates and associated Hill coefficients. Free energy changes between RNA device states are predicted from a standard RNA folding program, RNAStructure 4.2.

| Device | $\Delta\Delta G_{IG2}$ (kcal / mol) | $\Delta\Delta G_{IG1}$ (kcal / mol) | Degree of cooperativity or signal gain |
|---|---|---|---|
| **Non-cooperative** | | | |
| theo-theo-On1 | 0.3 | 0.3 | none |
| theo-theo-On2 | 2.8 | 0.3 | none |
| theo-theo-On3 | 1.8 | 0.3 | none |
| theo-theo-On4 | 1.9 | 0.3 | none |
| theo-theo-On5 | 0.0 | 0.3 | none |
| theo-theo-On6 | 0.9 | 0.3 | none |
| theo-theo-On7 | 3.0 | 0.3 | none |
| theo-theo-On8 | 2.8 | 0.3 | none |
| theo-theo-On9 | 2.9 | 0.0 | none |
| **Cooperative** | | | |
| theo-theo-On10 | 0.3 | 1.0 | $n_H \approx 1.32$ |
| theo-theo-On11 | 1 | 1.0 | $n_H \approx 1.63$ |
| theo-theo-On12 | 1.4 | 1.0 | $n_H \approx 1.47$ |
| theo-theo-On13 | 2.2 | 1.0 | $n_H \approx 1.65$ |


## Acknowledgements

We thank A. Babiskin for providing pRzS; Y. Chen and J. Liang for constructive suggestions in data analysis and presentation; and D. Endy for critical reading of the manuscript. This work was supported by the Center for Biological Circuit Design at Caltech (fellowship to M.N.W.), the Arnold and Mabel Beckman Foundation (grant to C.D.S.), and the National Institutes of Health (grant to C.D.S.).


## References


1. Endy, D. Foundations for engineering biology. Nature 438, 449-53 (2005).

2. Guet, C. C., Elowitz, M. B., Hsing, W. & Leibler, S. Combinatorial synthesis of genetic networks. Science 296, 1466-70 (2002).

3. Kramer, B. P., Fischer, C. & Fussenegger, M. BioLogic gates enable logical transcription control in mammalian cells. Biotechnol Bioeng 87, 478-84 (2004).

4. Cox, R. S., 3rd, Surette, M. G. & Elowitz, M. B. Programming gene expression with combinatorial promoters. Mol Syst Biol 3, 145 (2007).

5. Anderson, J. C., Voigt, C. A. & Arkin, A. P. Environmental signal integration by a modular AND gate. Mol Syst Biol 3, 133 (2007).

6. Breaker, R. R. Natural and engineered nucleic acids as tools to explore biology. Nature 432, 838-45 (2004).

7. Seelig, G., Soloveichik, D., Zhang, D. Y. & Winfree, E. Enzyme-free nucleic acid logic circuits. Science 314, 1585-8 (2006).

8. Dirks, R. M. & Pierce, N. A. Triggered amplification by hybridization chain reaction. Proc Natl Acad Sci U S A 101, 15275-8 (2004).

9. Stojanovic, M. N., Mitchell, T. E. & Stefanovic, D. Deoxyribozyme-based logic gates. J Am Chem Soc 124, 3555-61 (2002).

10. Stojanovic, M. N. & Stefanovic, D. Deoxyribozyme-based half-adder. J Am Chem Soc 125, 6673-6 (2003).

11. Stojanovic, M. N. & Stefanovic, D. A deoxyribozyme-based molecular automaton. Nat Biotechnol 21, 1069-74 (2003).

12. Benenson, Y. et al. Programmable and autonomous computing machine made of biomolecules. Nature 414, 430-4 (2001).

13. Benenson, Y., Gil, B., Ben-Dor, U., Adar, R. & Shapiro, E. An autonomous molecular computer for logical control of gene expression. Nature 429, 423-9 (2004).

14. Breaker, R. R. Engineered allosteric ribozymes as biosensor components. Curr Opin Biotechnol 13, 31-9 (2002).

15. Jose, A. M., Soukup, G. A. & Breaker, R. R. Cooperative binding of effectors by an allosteric ribozyme. Nucleic Acids Res 29, 1631-7 (2001).

16. Penchovsky, R. & Breaker, R. R. Computational design and experimental validation of oligonucleotide-sensing allosteric ribozymes. Nat Biotechnol 23, 1424-33 (2005).

17. Robertson, M. P. & Ellington, A. D. In vitro selection of an allosteric ribozyme that transduces analytes to amplicons. Nat Biotechnol 17, 62-6 (1999).

18. Isaacs, F. J., Dwyer, D. J. & Collins, J. J. RNA synthetic biology. Nat Biotechnol 24, 545-54 (2006).

19. Suess, B. & Weigand, J. E. Engineered riboswitches - Overview, Problems and Trends. RNA Biol 5 (2008).

20. Rinaudo, K. et al. A universal RNAi-based logic evaluator that operates in mammalian cells. Nat Biotechnol 25, 795-801 (2007).

21. Brown, B. D. et al. Endogenous microRNA can be broadly exploited to regulate transgene expression according to tissue, lineage and differentiation state. Nat Biotechnol 25, 1457-67 (2007).

22. Mathews, D. H. & Turner, D. H. Prediction of RNA secondary structure by free energy minimization. Curr Opin Struct Biol 16, 270-8 (2006).

23. Parisien, M. & Major, F. The MC-Fold and MC-Sym pipeline infers RNA structure from sequence data. Nature 452, 51-5 (2008).

24. Win, M. N. & Smolke, C. D. From the Cover: A modular and extensible RNA-based gene-regulatory platform for engineering cellular function. Proc Natl Acad Sci U S A 104, 14283-8 (2007).

25. Khvorova, A., Lescoute, A., Westhof, E. & Jayasena, S. D. Sequence elements outside the hammerhead ribozyme catalytic core enable intracellular activity. Nat Struct Biol 10, 708-12 (2003).

26. Welz, R. & Breaker, R. R. Ligand binding and gene control characteristics of tandem riboswitches in Bacillus anthracis. Rna 13, 573-82 (2007).

27. Sudarsan, N. et al. Tandem riboswitch architectures exhibit complex gene control functions. Science 314, 300-4 (2006).

28. Nelson, D. L. & Cox, M. M. Lehninger Principles of Biochemistry (W. H. Freeman and Company, New York, 2005).

29. Mandal, M. et al. A glycine-dependent riboswitch that uses cooperative binding to control gene expression. Science 306, 275-9 (2004).

30. Woodside, M. T. et al. Nanomechanical measurements of the sequence-dependent folding landscapes of single nucleic acid hairpins. Proc Natl Acad Sci U S A 103, 6190-5 (2006).

31. Tuerk, C. & Gold, L. Systematic evolution of ligands by exponential enrichment: RNA ligands to bacteriophage T4 DNA polymerase. Science 249, 505-10 (1990).

32. Ellington, A. D. & Szostak, J. W. In vitro selection of RNA molecules that bind specific ligands. Nature 346, 818-22 (1990).

33. Sambrook, J. & Russell, D. W. Molecular cloning: a laboratory manual (Cold Spring Harbor Laboratory Press, Cold Spring Harbor, NY, 2001).

34. Mateus, C. & Avery, S. V. Destabilized green fluorescent protein for monitoring dynamic changes in yeast gene expression with flow cytometry. Yeast 16, 1313-23 (2000).

35. Gietz, R. & Woods, R. in Guide to Yeast Genetics and Molecular and Cell Biology, Part B. (eds. Guthrie, C. & Fink, G.) 87-96 (Academic Press, San Diego, 2002).

36. Yokobayashi, Y., Weiss, R. & Arnold, F. H. Directed evolution of a genetic circuit. Proc Natl Acad Sci U S A 99, 16587-91 (2002).

37. Basu, S., Mehreja, R., Thiberge, S., Chen, M. T. & Weiss, R. Spatiotemporal control of gene expression with pulse-generating networks. Proc Natl Acad Sci U S A 101, 6355-60 (2004).

38. Levine, E., Zhang, Z., Kuhlman, T. & Hwa, T. Quantitative characteristics of gene regulation by small RNA. PLoS Biol 5, e229 (2007).

39. Hebert, S. S. et al. Loss of microRNA cluster miR-29a/b-1 in sporadic Alzheimer's disease correlates with increased BACE1/beta-secretase expression. Proc Natl Acad Sci U S A 105, 6415-20 (2008).

40. Calin, G. A. et al. MiR-15a and miR-16-1 cluster functions in human leukemia. Proc Natl Acad Sci U S A 105, 5166-71 (2008).

41. Ventura, A. et al. Targeted deletion reveals essential and overlapping functions of the miR-17 through 92 family of miRNA clusters. Cell 132, 875-86 (2008).

42. Soukup, G. A., Emilsson, G. A. & Breaker, R. R. Altering molecular recognition of RNA aptamers by allosteric selection. J Mol Biol 298, 623-32 (2000).

43. Rodionov, D. A., Dubchak, I., Arkin, A., Alm, E. & Gelfand, M. S. Reconstruction of regulatory and metabolic pathways in metal-reducing delta-proteobacteria. Genome Biol 5, R90 (2004).

44. Deans, T. L., Cantor, C. R. & Collins, J. J. A tunable genetic switch based on RNAi and repressor proteins for regulating gene expression in mammalian cells. Cell 130, 363-72 (2007).